5

Green's Functions for Tight-Binding Hamiltonians

Summary. We introduce the so-called tight-binding Hamiltonians (TBH), which have the form

$$\mathcal{H} = \sum_{\boldsymbol{\ell}} |\boldsymbol{\ell}\rangle\, \varepsilon_{\boldsymbol{\ell}}\, \langle\boldsymbol{\ell}| + \sum_{\boldsymbol{\ell}\boldsymbol{m}} |\boldsymbol{\ell}\rangle\, V_{\boldsymbol{\ell}\boldsymbol{m}}\, \langle\boldsymbol{m}| \ ,$$

where each state $|\boldsymbol{\ell}\rangle$ is an atomiclike orbital centered at the site $\boldsymbol{\ell}$; the sites $\{\boldsymbol{\ell}\}$ form a lattice. Such Hamiltonians are very important in solid-state physics. Here we calculate the Green's functions associated with the TBH for various simple lattices. We also review briefly some applications in solid-state physics.

5.1 Introductory Remarks

In this chapter we examine the Green's functions associated with a class of *periodic* Hamiltonians, i.e., Hamiltonians remaining invariant under a translation by any vector $\boldsymbol{\ell}$, where $\{\boldsymbol{\ell}\}$ form a regular lattice in d-dimensional space

$$\boldsymbol{\ell} = \sum_{a=1}^{d} \ell_a \boldsymbol{r}_a \ , \quad \ell_a = 0\ , \pm 1, \pm 2, \ldots \tag{5.1}$$

and $\boldsymbol{r}_a$ $(a = 1, \ldots, d)$ are d linear independent vectors forming the basis of the lattice.

The reasons for considering here periodic Hamiltonians are the following.

1. They produce continuous spectra that possess not only a lower bound, as in the free-particle case, but an *upper* bound (or bounds) as well. Thus, the physics is not only richer but more symmetric and in some sense more satisfying.
2. They are of central importance for understanding the electronic behavior of perfect crystalline solids.
3. They provide the basis for understanding the electronic properties of real, imperfect crystalline solids, since the imperfections can be treated as a perturbation $\mathcal{H}_1$ using techniques developed in Chap. 4.

4. They are mathematically equivalent to a system of coupled 1-d harmonic oscillators and, as a result, they describe (by direct generalization to 3-d) the ionic motions in a crystalline solid. Furthermore, imperfections can be treated by techniques presented in Chap. 4.
5. The class of simplified periodic Hamiltonians we consider here allows us to obtain simple closed-form results for certain perturbation problems. Thus the physics presented in Sect. 4.1 can be better appreciated without the burden of a complicated algebra. This point will be examined in detail in the next chapter.

Before we introduce the class of Hamiltonians under consideration, we remind the reader of some of the basic properties of the eigenfunctions and eigenvalues of a periodic Hamiltonian [22–30].

The eigenfunctions, which are called *Bloch functions*, are plane wavelike, i.e.,

$$\psi_{n\boldsymbol{k}}(\boldsymbol{r}) = \frac{1}{\sqrt{\Omega}} \mathrm{e}^{\mathrm{i}\boldsymbol{k}\cdot\boldsymbol{r}} u_{n\boldsymbol{k}}(\boldsymbol{r}) \ , \tag{5.2}$$

where the preexponential $u_{n\boldsymbol{k}}(\boldsymbol{r})$ is not a constant, as in the genuine plane waves, but a periodic function of $\boldsymbol{r}$ of the same periodicity as the potential; the quantum number $\boldsymbol{k}$ determines how much the phase changes when we propagate by a lattice vector $\boldsymbol{\ell}$:

$$\psi_{n\boldsymbol{k}}(\boldsymbol{r}+\boldsymbol{\ell}) = \mathrm{e}^{\mathrm{i}\boldsymbol{k}\cdot\boldsymbol{\ell}} \psi_{n\boldsymbol{k}}(\boldsymbol{r}) \ . \tag{5.3}$$

Note that the quantity $\boldsymbol{k}$ is restricted to a finite region in $\boldsymbol{k}$-space, called the *first Brillouin zone*. The other quantum number n, which is called the *band index*, takes integer values; the presence of n compensates somehow the restriction of $\boldsymbol{k}$ in the first Brillouin zone. It is worthwhile to stress that eigenstates of the type (5.2) imply propagation without any resistance similar (but not identical) to the free-particle case.

Periodicity has more profound and characteristic effects on the energy spectrum, which consists of continua, called *bands*, that may or may not overlap; there are also energy regions, called *gaps*, which do not belong to any band and, as a result, correspond to zero density of states. The boundary points between bands and gaps are called *band edges*. The eigenenergies $E_n(\boldsymbol{k})$ are continuous functions of $\boldsymbol{k}$ within each band n. The band edges correspond to absolute minima or maxima of E vs. $\boldsymbol{k}$ for a given n or a set $\{n\}$ of overlapping bands.

There are two simple diametrically opposite starting points for obtaining the electronic eigenenergies, $E_n(\boldsymbol{k})$, and the eigenfunctions, $\psi_{n\boldsymbol{k}}(\boldsymbol{r})$, in crystalline solids.

One, the nearly-free electron (NFE) model, takes the point of view that in a solid the total *effective* potential felt by each electron is weak enough to be treated by perturbation methods (the unperturbed solutions being plane waves). Developments based on this approach led to the pseudopotential

method, which was proven to be very fruitful indeed, especially for simple metals and semiconductors [31–38].

The other approach views the solids as being made up of atoms brought together from an infinite relative distance. It is then natural (following the usual practice for molecules) to try to express the unknown electronic wave functions as linear combinations of atomic orbitals (LCAO). In this chapter we shall deal with the simpler possible version of this approach by considering only one atom per primitive crystal cell, only one atomic orbital per atom, nearest-neighbor coupling only, and orthonormality of the atomic orbitals. We shall refer to this oversimplified version of the LCAO as the tight-binding model (TBM); the atomic orbital associated with the atom located at site $\boldsymbol{\ell}$ will be symbolized by

$$w(\boldsymbol{r} - \boldsymbol{\ell}) = \langle \boldsymbol{r} \,|\, \boldsymbol{\ell} \rangle \ . \tag{5.4}$$

For more realistic calculations one needs to take into account several complicating factors:

1. Usually one needs several orbitals per atom, e.g., tetrahedral solids (C, Si, Ge, etc.) require at least four orbitals per site (one s-like and three p-like), while transition metals require in addition five d-like orbitals. Furthermore, one may need to employ hybrid atomic orbitals, or modified, atomiclike orbitals such as Wannier functions (see Appendix E).
2. One may have more than one atom per primitive crystalline cell.
3. The matrix elements between orbitals at different sites may not decay fast enough so that more than nearest-neighbor matrix elements may be needed.
4. The atomiclike orbitals at different sites may not be orthogonal to each other. Indeed, true atomic orbitals are not orthogonal.

Note that there is freedom in choosing the atomiclike orbitals. The Wannier functions, mentioned before (Appendix E), are one possible choice; it has the advantage of orthonormality and completeness and the disadvantage of weak decay (and hence many appreciable matrix elements). One may employ this freedom in choosing the basis so as to simplify the problem, i.e., to reduce the number of appreciable matrix elements and facilitate their computation.

The direct calculation of the matrix elements in this atomiclike orbital basis is in general a very difficult task. To obtain them indirectly one fits the LCAO results to either alternative calculations (see, e.g., [39]) or to experimental data (see, e.g., [40–42]). Harrison [25, 26, 43, 44] obtained very simple, general, and more or less acceptable (but not accurate) expressions for the matrix elements by requiring that the NFE and the LCAO methods produce consistent results. Slater and Koster [45] were the first to study in detail the dependence of the off-diagonal matrix elements on the orientation of the orbitals relative to the vector joining two neighboring atoms. As shown in Harrison's book [25], the LCAO method is a very useful tool for analyzing many classes of materials such as covalent solids [39,46–52], ionic solids [53], simple

metals [54], transition metals [55–57], transition-metal compounds [58–61], the A15 (such as Nb_3Sn) compounds [62,63], high T_c oxide superconductors (such as $YBa_2Cu_3O_7$) [64], etc.

5.2 The Tight-Binding Hamiltonian (TBH)

As was mentioned in Sect. 5.1, the basic set of functions within the TBM consists of orthonormal, identical, atomiclike orbitals, each one centered at the lattice sites $\boldsymbol{\ell} = \ell_1 \boldsymbol{r}_1 + \ell_2 \boldsymbol{r}_2 + \ell_3 \boldsymbol{r}_3$ (for $d = 3$), where each ℓ_i takes all integer values; thus $\langle \boldsymbol{r} \,|\, \boldsymbol{\ell} \rangle = w(\boldsymbol{r} - \boldsymbol{\ell})$. The matrix elements of the Hamiltonian within this subspace are

$$\langle \boldsymbol{\ell} \,|\, \mathcal{H} \,|\, \boldsymbol{m} \rangle = \varepsilon_{\boldsymbol{\ell}} \delta_{\boldsymbol{\ell m}} + V_{\boldsymbol{\ell m}} \; . \tag{5.5}$$

Following the usual notation we have denoted the diagonal matrix elements by $\varepsilon_{\boldsymbol{\ell}}$ and the off-diagonal matrix elements by $V_{\boldsymbol{\ell m}}$ ($V_{\boldsymbol{\ell\ell}} \equiv 0$).

The periodicity of the Hamiltonian, i.e., its invariance under translations by a lattice vector $\boldsymbol{\ell}$, implies that

$$\varepsilon_{\boldsymbol{\ell}} = \varepsilon_0 \qquad \text{for all } \boldsymbol{\ell} \; , \tag{5.6a}$$

$$V_{\boldsymbol{\ell m}} = V_{\boldsymbol{\ell} - \boldsymbol{m}} \; . \tag{5.6b}$$

It should be stressed that the Hamiltonian, which describes a real periodic solid, has matrix elements outside the subspace spanned by the $|\boldsymbol{\ell}\rangle$ vectors and that this subspace is coupled with the rest of the Hilbert space. Nevertheless, we restrict ourselves to this subspace for the sake of simplicity. The price for this approximation can be considered reasonable, since many important *qualitative* features are retained in spite of this drastic simplification. Furthermore, bands arising from atomic orbitals weakly overlapping with their neighbors (i.e., tightly bound to their atoms) can be described rather accurately by working within the above-defined subspace or its straightforward generalization [22,25,28]. For this reason, the Hamiltonian (5.5), which is confined within the subspace spanned by $\{|\boldsymbol{\ell}\rangle\}$, where $\boldsymbol{\ell}$ runs over all lattice sites, is called the tight-binding Hamiltonian (TBH) or the tight-binding model (TBM).

The TBH, (5.5), can be written equivalently as

$$\mathcal{H} = \sum_{\boldsymbol{\ell}} |\boldsymbol{\ell}\rangle \, \varepsilon_{\boldsymbol{\ell}} \, \langle \boldsymbol{\ell}| + \sum_{\boldsymbol{\ell m}} |\boldsymbol{\ell}\rangle \, V_{\boldsymbol{\ell m}} \, \langle \boldsymbol{m}| \; , \qquad V_{\boldsymbol{\ell\ell}} = 0 \; , \tag{5.7}$$

where $\varepsilon_{\boldsymbol{\ell}}$ and $V_{\boldsymbol{\ell m}}$ satisfy (5.6a) and (5.6b). We shall also consider the more general case where the lattice can be divided into two interpenetrating sublattices such that each point of sublattice 1 is surrounded by points belonging to sublattice 2; the Hamiltonian remains invariant under translation by vectors of sublattice 1 or sublattice 2. In this case

$$\varepsilon_{\boldsymbol{\ell}} = \begin{cases} \varepsilon_1 & \text{if } \boldsymbol{\ell} \text{ belongs to sublattice 1} \; , \qquad (5.8a) \\ \varepsilon_2 & \text{if } \boldsymbol{\ell} \text{ belongs to sublattice 2} \; . \qquad (5.8b) \end{cases}$$

For the sake of simplicity we assume in our explicit results that

$$V_{\boldsymbol{\ell m}} = \begin{cases} V, & \boldsymbol{\ell}, \boldsymbol{m} \text{ nearest neighbors}, \quad (5.9a) \\ 0, & \text{otherwise}. \quad (5.9b) \end{cases}$$

This last assumption, although not necessary, simplifies the calculational effort. The set $\{|\boldsymbol{\ell}\rangle\}$ is assumed orthonormal:

$$\langle \boldsymbol{\ell} \,|\, \boldsymbol{m} \rangle = \delta_{\boldsymbol{\ell m}} \,. \tag{5.10}$$

Thus a TBH is characterized by:

1. The lattice structure associated with the points $\{\boldsymbol{\ell}\}$.
2. The values of the diagonal matrix element $\{\varepsilon_{\boldsymbol{\ell}}\}$; in the simple periodic case, where (5.6a) is satisfied, there is only one common value that can be taken as zero by a proper redefinition of the origin of energy; in the two-sublattice periodic case, where (5.8) is satisfied, the quantity of physical significance is the difference $\varepsilon_1 - \varepsilon_2 > 0$.
3. The off-diagonal matrix elements $V_{\boldsymbol{\ell m}}$, which in the periodic case depend only on the difference $\boldsymbol{\ell} - \boldsymbol{m}$.

If the simplifying assumption (5.9) is made, there is only one quantity, V, which, following the usual practice in the literature, can be taken as negative (for s-like orbitals V is indeed negative; for p- or d-orbitals the sign and the magnitude of V depends on the relative orientation of the orbitals with respect to the direction of the line joining the two neighboring atoms). It must be pointed out that a negative V, in contrast to a positive V, preserves the well-known property that as the energy of real eigenfunctions increases so does the number of their sign alternation. In any case one can obtain the positive V Green's functions from those calculated here by employing the relation

$$G(\boldsymbol{\ell}, \boldsymbol{m}; E + \mathrm{i}s, \{\varepsilon_\ell\}, V) = -G(\boldsymbol{\ell}, \boldsymbol{m}; -E - \mathrm{i}s, \{-\varepsilon_\ell\}, -V) \,. \tag{5.11}$$

The first term on the rhs of (5.7) describes a particle that can be trapped around any particular lattice site $\boldsymbol{\ell}$ with an eigenenergy $\varepsilon_{\boldsymbol{\ell}}$. The second term allows the particle to hop from site $\boldsymbol{\ell}$ to site $\boldsymbol{m}$ with a transfer matrix element $V_{\boldsymbol{\ell m}}$. The quantum motion associated with the Hamiltonian (5.7) is equivalent to the wave motion of the coupled pendula shown in Fig. 5.1. This can easily be seen by writing the time-independent Schrödinger equation $\mathcal{H}\,|\psi\rangle = E\,|\psi\rangle$ as

$$(\varepsilon_{\boldsymbol{i}} - E)\, c_{\boldsymbol{i}} + \sum_{\boldsymbol{j}} V_{\boldsymbol{ij}} c_{\boldsymbol{j}} = 0 \,, \tag{5.12}$$

where $|\psi\rangle = \sum_{\boldsymbol{i}} c_{\boldsymbol{i}}\,|\boldsymbol{i}\rangle$ and (5.7) and (5.10) are used. The equations of motion of the coupled pendula are

$$\left(m_{\boldsymbol{i}} \omega_{\boldsymbol{i}}^2 + \sum_{\boldsymbol{j}} \kappa_{\boldsymbol{ij}} - m_{\boldsymbol{i}} \omega^2 \right) u_{\boldsymbol{i}} - \sum_{\boldsymbol{j}} \kappa_{\boldsymbol{ij}} u_{\boldsymbol{j}} = 0 \,, \tag{5.13}$$

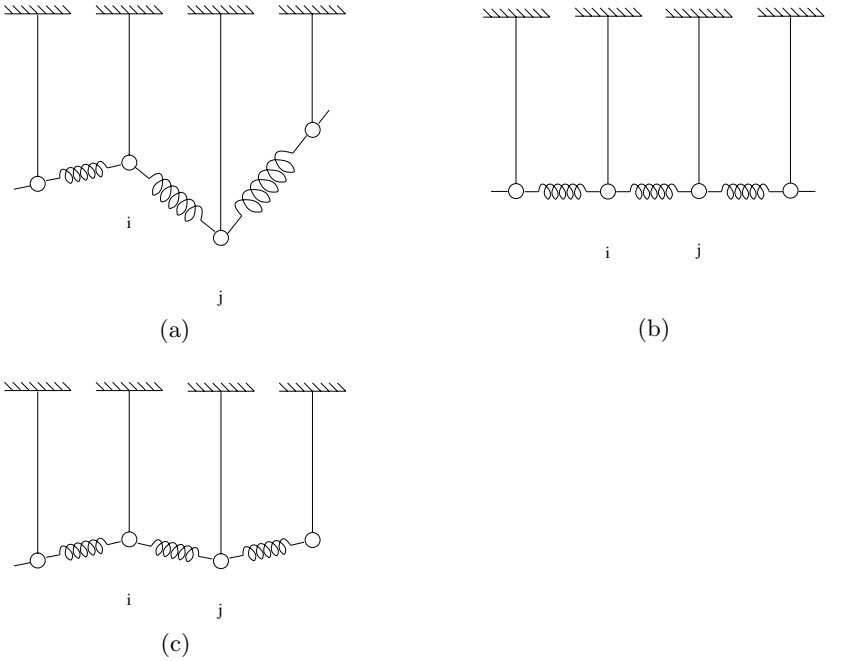

Fig. 5.1. One-dimensional coupled pendulum analog of the tight-binding Hamiltonian. Only nearest-neighbor couplings are shown (**a**). In the periodic case examined in this chapter, all pendula and all nearest-neighbor couplings are identical (**b**). The double spacing periodic case is also shown (**c**)

or

$$\left(\omega_{\boldsymbol{i}}^2 + \frac{1}{m_{\boldsymbol{i}}}\sum_{\boldsymbol{ij}}\kappa_{\boldsymbol{ij}} - \omega^2\right) u_{\boldsymbol{i}} - \frac{1}{m_{\boldsymbol{i}}}\sum_{\boldsymbol{ij}}\kappa_{\boldsymbol{ij}} u_{\boldsymbol{j}} = 0\ , \qquad (5.13')$$

where $u_{\boldsymbol{i}}$ is the 1-d displacement of the pendulum located at site $\boldsymbol{i}$, $\omega_{\boldsymbol{i}}$ is its eigenfrequency in the absence of coupling, and $-\sum_{\boldsymbol{j}} k_{\boldsymbol{ij}}\,(u_{\boldsymbol{i}} - u_{\boldsymbol{j}})$ is the force exercised on the pendulum at the $\boldsymbol{i}$ site as a result of the couplings with all the other pendula; $m_{\boldsymbol{i}}$ is the mass at $\boldsymbol{i}$. The correspondence between the electronic and the pendulum case is illustrated in Table 5.1.

The simple mechanical system of coupled pendula is very important for solid-state physics: through the analogies in Table 5.1, it allows us to introduce the basic features of electronic behavior in crystalline solids and to obtain a clear physical picture of electronic propagation in periodic media. (Actually F. Bloch arrived at his famous explanation of almost unimpeded electronic propagation in crystalline metals by recalling the free propagation of motion in a periodic 1-d array of coupled pendula.) Furthermore, if we generalize to 3-d displacements, the problem of coupled pendula is reduced to that of the ionic (or atomic) motion in solids (by setting $\omega_i = 0$) since each ion (or atom)

Table 5.1. Analogy between the TBH and a system of coupled pendula

Electronic case	**Pendulum case**
$c_{\boldsymbol{i}}$: component of eigenfunction at site $\boldsymbol{i}$	$u_{\boldsymbol{i}}$: displacement of pendulum located at site $\boldsymbol{i}$
$-V_{\boldsymbol{ij}}$: minus transfer matrix element between $\lvert\boldsymbol{i}\rangle$ and $\lvert\boldsymbol{j}\rangle$	$\kappa_{\boldsymbol{ij}}/m_{\boldsymbol{i}}$: spring constant coupling pendula at sites $\boldsymbol{i}$ and $\boldsymbol{j}$ over mass $m_{\boldsymbol{i}}$
E: eigenenergy	ω^2: square of eigenfrequency
$\varepsilon_{\boldsymbol{i}}$: site energy	$\omega_i^2 + 1/m_{\boldsymbol{i}} \sum_{\boldsymbol{j}} \kappa_{\boldsymbol{ij}}$: square of uncoupled eigenfrequency plus sum of spring constants connected to $\boldsymbol{i}$ over mass $m_{\boldsymbol{i}}$

is indeed performing small oscillations around its equilibrium position with the restoring force being equal to $-\sum_j \boldsymbol{k}_{ij}\,(\boldsymbol{u}_i - \boldsymbol{u}_j)$. Thus for the periodic ($m_i = m_0$, $\omega_i = \omega_0$, and $\kappa_{\boldsymbol{ij}} = \kappa_{\boldsymbol{i}-\boldsymbol{j}}$) case, the solution of system (5.13′) is, according to (5.3):

$$u_{\boldsymbol{j}} = u_{\boldsymbol{i}} \mathrm{e}^{\mathrm{i}\boldsymbol{k}\cdot(\boldsymbol{j}-\boldsymbol{i})}\ , \quad \text{for each pair } \boldsymbol{i}, \boldsymbol{j}\ , \tag{5.14a}$$

and then

$$\omega^2(\boldsymbol{k}) = \omega_0^2 + \frac{1}{m_0}\sum_{\boldsymbol{j}} \kappa_{0\boldsymbol{j}} - \frac{1}{m_0}\sum_{\boldsymbol{j}} \kappa_{0\boldsymbol{j}} \mathrm{e}^{\mathrm{i}\boldsymbol{k}\cdot\boldsymbol{j}}\ . \tag{5.14b}$$

The reader may verify by direct substitution that (5.14a) and (5.14b) satisfy the system of equations (5.13′).

Setting $\boldsymbol{i} = 0$ in (5.14a), replacing the dummy index $\boldsymbol{j}$ by $\boldsymbol{\ell}$, and using the analogies in Table 5.1, we find for the electronic eigenfunctions and eigenenergies of the TBM:

$$|\boldsymbol{k}) = \sum_{\boldsymbol{\ell}} c_{\boldsymbol{\ell}}\,|\boldsymbol{\ell}\rangle = c_0 \sum_{\boldsymbol{\ell}} \mathrm{e}^{\mathrm{i}\boldsymbol{k}\cdot\boldsymbol{\ell}}\,|\boldsymbol{\ell}\rangle\ , \tag{5.15a}$$

$$E(\boldsymbol{k}) = \varepsilon_0 + \sum_{\boldsymbol{\ell}} V_{0\boldsymbol{\ell}} \mathrm{e}^{\mathrm{i}\boldsymbol{k}\cdot\boldsymbol{\ell}}\ , \tag{5.15b}$$

where the orthonormality of the eigenstates $\{|\boldsymbol{k})\}$ imply that $c_0 = 1/\sqrt{N}$.

Equation (5.15a) means that the eigenmodes are propagating waves such that the amplitude at each site is the same and the phase changes in a regular

way: $\phi_{\boldsymbol{\ell}} = \boldsymbol{k} \cdot \boldsymbol{\ell}$. To obtain explicit results, we employ the simplifying equation (5.9) so that (5.15b) becomes

$$E(\boldsymbol{k}) = \varepsilon_0 + V \sum_{\boldsymbol{\ell}}{}' \mathrm{e}^{\mathrm{i}\boldsymbol{k} \cdot \boldsymbol{\ell}} , \tag{5.16}$$

where the summation extends over the sites neighboring the origin. For the 1-d case we have

$$E(k) = \varepsilon_0 + 2V \cos(ka) , \quad \text{1-d} , \tag{5.17}$$

where a is the lattice constant. For a 2-d square lattice

$$E(\boldsymbol{k}) = \varepsilon_0 + 2V \left[\cos(k_1 a) + \cos(k_2 a)\right] , \quad \text{2-d square.} \tag{5.18}$$

For the 3-d simple cubic we have

$$E(\boldsymbol{k}) = \varepsilon_0 + 2V \left[\cos(k_1 a) + \cos(k_2 a) + \cos(k_3 a)\right] , \quad \text{3-d simple cubic.} \tag{5.19}$$

In Fig. 5.2 we plot E vs. k for the 1-d case; k is restricted within the first Brillouin zone, which for the 1-d case extends from $-\pi/a$ to π/a. The function $E(k)$ has an absolute maximum (which corresponds to the upper band edge) for $k = \pi/a$ or $-\pi/a$ with a value $E_{\max} = \varepsilon_0 + 2\,|V|$; it has an absolute minimum (which corresponds to a lower band edge) for $k = 0$ with a value $E_{\min} = \varepsilon_0 - 2\,|V|$. Thus the spectrum is a continuum (a band) extending from $\varepsilon_0 - 2\,|V|$ to $\varepsilon_0 + 2\,|V|$. The bandwidth is $4\,|V|$. One can easily show that cases (5.17) to (5.19) produce a single band extending from $\varepsilon_0 - Z\,|V|$ to

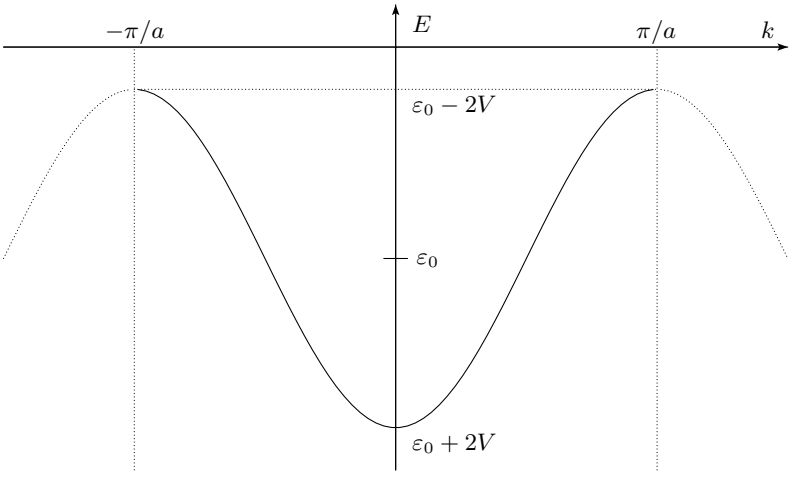

Fig. 5.2. E vs. k for the 1-d tight-binding case with nearest-neighbor coupling $V(< 0)$). $B = 2\,|V|$ is half the bandwidth

$\varepsilon_0 + Z\,|V|$, where Z is the number of nearest neighbors. The quantity $Z\,|V|$, which is equal to half the bandwidth, is usually symbolized by B. For 2-d and 3-d cases the functions $E(\boldsymbol{k})$ are presented either by plotting E vs. $\boldsymbol{k}$ as $\boldsymbol{k}$ varies along chosen directions or by plotting the lines (2-d case) or surfaces (3-d case) of constant energy (Figs. 5.3–5.5). In all cases $\boldsymbol{k}$ is restricted within the first Brillouin zone.

For a 1-d periodic model of ionic vibration we obtain from (5.14b) (by setting $\omega_0 = 0$ and assuming only nearest-neighbor couplings) the following result:

$$m_0\omega^2(k) = 2\kappa\,[1 - \cos(ka)] = 4\kappa \sin^2\left(\frac{ka}{2}\right)\,, \tag{5.20a}$$

or

$$\omega(k) = 2\sqrt{\frac{\kappa}{m_0}}\left|\sin\left(\frac{ka}{2}\right)\right| \underset{k\to 0}{\longrightarrow} \sqrt{\frac{\kappa a}{\varrho}}k\,, \tag{5.20b}$$

where $\varrho = m_0/a$ is the average linear density and $\kappa a = B_m$ is the bulk modulus for the 1-d case. The quantity $\sqrt{B_m/\varrho}$ is the phase or group sound velocity for $ka \ll 1$. As ka approaches π, the phase velocity, ω/k, and the group velocity, $v_g \equiv \mathrm{d}\omega/\mathrm{d}k$, are different with $v_g \to 0$ as $ka \to \pi$.

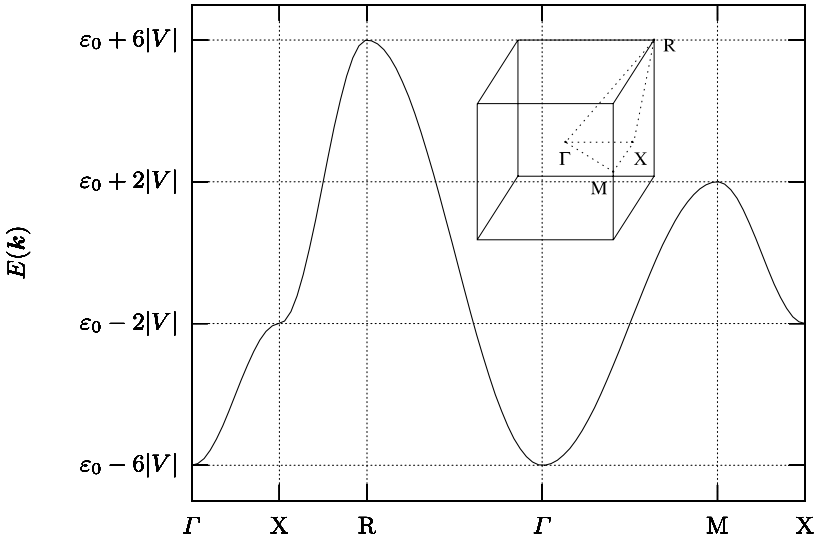

Fig. 5.3. E vs. $\boldsymbol{k}$ for 3-d simple cubic tight-binding case with nearest-neighbor coupling $V(< 0)$, as $\boldsymbol{k}$ varies along the straight-line segments of the first Brillouin zone (1BZ) shown in the insert

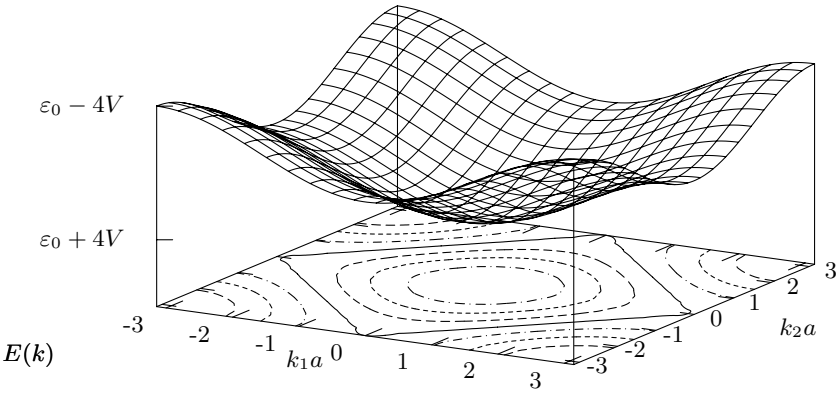

Fig. 5.4. Two-dimensional plot of E vs. $\boldsymbol{k}$ according to (5.18) ($V < 0$). The first Brillouin zone (1BZ) is the square $-\pi < k_1a,\, k_2a \leq \pi$. The contours of equal energy are also shown within the 1BZ

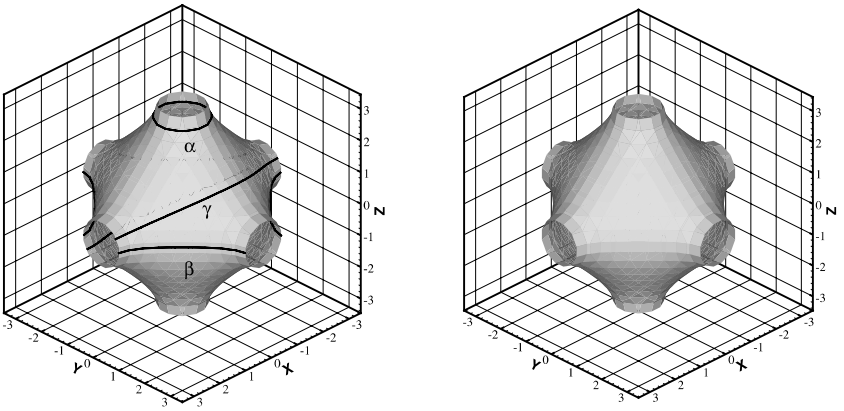

Fig. 5.5. Surface of constant energy $[E(\boldsymbol{k}) = \varepsilon_0 + 1.5V]$ in $\boldsymbol{k}$-space for the case of (5.19). The 1BZ (shown) is the cube $-\pi < k_1a,\, k_2a,\, k_3a \leq \pi$; the lines α, β, γ are intersections of this surface by various planes, and they give the semiclassical electronic trajectories in the presence of a static magnetic field perpendicular to each plane

5.3 Green's Functions

The Green's function for the TBH examined in the previous section is

$$G(z) = \sum_{\boldsymbol{k}} \frac{|\boldsymbol{k})\,(\boldsymbol{k}|}{z - E\,(\boldsymbol{k})}\ , \tag{5.21}$$

where $|\boldsymbol{k})$ is given by (5.15a) and $E\,(\boldsymbol{k})$ by (5.16). The matrix elements of $G(z)$ are

$$\begin{aligned} G\,(\boldsymbol{\ell}, \boldsymbol{m}; z) \equiv \langle \boldsymbol{\ell}\,|\,G(z)\,|\,\boldsymbol{m}\rangle &= \sum_{\boldsymbol{k}} \frac{\langle \boldsymbol{\ell}|\boldsymbol{k})\ (\boldsymbol{k}|\boldsymbol{m}\rangle}{z - E\,(\boldsymbol{k})} \\ &= \frac{\Omega}{N(2\pi)^d} \int_{1\mathrm{BZ}} \mathrm{d}\boldsymbol{k} \frac{\mathrm{e}^{\mathrm{i}\boldsymbol{k}\,\cdot\,(\boldsymbol{\ell}-\boldsymbol{m})}}{z - E\,(\boldsymbol{k})}\ , \end{aligned} \tag{5.22}$$

where the symbol 1BZ denotes that the integration must be restricted within the first Brillouin zone. In particular, all diagonal matrix elements are equal to each other and are given by

$$G\,(\boldsymbol{\ell}, \boldsymbol{\ell}; z) = \frac{\Omega}{N(2\pi)^d} \int_{1\mathrm{BZ}} \frac{\mathrm{d}\boldsymbol{k}}{z - E\,(\boldsymbol{k})}\ . \tag{5.23}$$

For large z one can omit $E\,(\boldsymbol{k})$ in the denominator of the integrand in (5.23) so that

$$G\,(\boldsymbol{\ell}, \boldsymbol{\ell}; z) \underset{z\to\infty}{\longrightarrow} \frac{1}{z} \frac{\Omega}{N(2\pi)^d} \int_{1\mathrm{BZ}} \mathrm{d}\boldsymbol{k}\ .$$

The volume of the first Brillouin zone equals $(2\pi)^d/\Omega_0$, where $\Omega_0 = \Omega/N$ is the volume of the primitive cell of the lattice. Hence,

$$G\,(\boldsymbol{\ell}, \boldsymbol{\ell}; z) \underset{z\to\infty}{\longrightarrow} \frac{1}{z}\ . \tag{5.24}$$

This behavior can be understood if one expresses $G\,(\boldsymbol{\ell}, \boldsymbol{\ell}; z)$ in terms of the density of states per site $\varrho(E)$

$$G\,(\boldsymbol{\ell}, \boldsymbol{\ell}; z) = \int \frac{\varrho(E)}{z - E} \mathrm{d}E \underset{z\to\infty}{\longrightarrow} \frac{1}{z} \int \varrho(E) \mathrm{d}E\ ; \tag{5.25}$$

but $\int \varrho(E) \mathrm{d}E = 1$ since there is one state per site. Below we give some explicit results for the various matrix elements of G for several lattices.

5.3.1 One-Dimensional Lattice

Substituting (5.17) into (5.22) we obtain (taking into account that $L/N = a$)

$$G(\ell, m; z) = \frac{L}{2\pi N} \int_{-\pi/a}^{\pi/a} \mathrm{d}k \frac{\mathrm{e}^{\mathrm{i}ka(\ell-m)}}{z - \varepsilon_0 - 2V\cos(ka)}$$

$$= \frac{1}{2\pi} \int_{-\pi}^{\pi} \mathrm{d}\phi \frac{\mathrm{e}^{\mathrm{i}\phi(\ell-m)}}{z - \varepsilon_0 - 2V\cos\phi} , \qquad \phi = ka . \tag{5.26}$$

To evaluate the integral, we observe first that it depends on the absolute value $|\ell - m|$. Next we transform it into an integral over the complex variable $w = \mathrm{e}^{\mathrm{i}\phi}$ along the unit circle. Thus we have

$$G(\ell, m; z) = \frac{1}{2\pi\mathrm{i}\,|V|} \oint \mathrm{d}w \frac{w^{|\ell-m|}}{w^2 + 2xw + 1} , \tag{5.27}$$

where

$$x = \frac{z - \varepsilon_0}{B} , \qquad B = 2\,|V| . \tag{5.28}$$

The two roots of $w^2 + 2xw + 1 = 0$ are given by

$$\varrho_1 = -x + \sqrt{x^2 - 1} , \tag{5.29a}$$

$$\varrho_2 = -x - \sqrt{x^2 - 1} , \tag{5.29b}$$

where by $\sqrt{x^2 - 1}$ we denote the square root whose imaginary part has the same sign as $\mathrm{Im}\{x\}$. (For real x one has to follow a limiting procedure.) It follows that $\varrho_1\varrho_2 = 1$. One can show that $|\varrho_1| < 1$ and $|\varrho_2| > 1$ unless x is real and satisfies the relation $-1 \le x \le 1$. In the latter case both roots lie on the unit circle, and the integral (5.27) is not well defined. Hence, this condition gives the continuous spectrum of $\mathcal{H}$ which lies in the real E-axis between $\varepsilon_0 - 2\,|V|$ and $\varepsilon_0 + 2\,|V|$. For z not coinciding with this singular line, we obtain for $G(\ell, m; z)$ by the method of residues

$$G(\ell, m; z) = \frac{1}{|V|} \frac{\varrho_1\,|\ell - m|}{\varrho_1 - \varrho_2} = \frac{1}{\sqrt{(z - \varepsilon_0)^2 - B^2}} \varrho_1^{|\ell-m|} , \tag{5.30}$$

where ϱ_1 is given by (5.29a). For z coinciding with the spectrum we have

$$G^{\pm}(\ell, m; E) = \frac{\mp\mathrm{i}}{\sqrt{B^2 - (E - \varepsilon_0)^2}} \left(-x \pm \mathrm{i}\sqrt{1 - x^2}\right)^{|\ell-m|} , \tag{5.31}$$

where $\varepsilon_0 - B \le E \le \varepsilon_0 + B$, $x = (E - \varepsilon_0)/B$ and the symbol $\sqrt{1 - x^2}$ denotes the positive square root.

The density of states per site is given by

$$\varrho(E) = \mp\frac{1}{\pi}\mathrm{Im}\left\{G^{\pm}(\ell,\ell;E)\right\} = \frac{\theta\left(B-|E-\varepsilon_0|\right)}{\pi\sqrt{B^2-\left(E-\varepsilon_0\right)^2}}\,. \tag{5.32}$$

In Fig. 5.6 we plot the real and the imaginary part of the diagonal matrix element $G(\ell,\ell;E)$ vs. E Notice the square root singularities at both band edges. As was mentioned in Chap. 3, this behavior is characteristic of one-dimensionality. Note that the off-diagonal matrix elements $G(\ell,m;z)$ decay exponentially with the distance $|\ell-m|$ when z does not coincide with the spectrum. On the other hand, when z belongs to the spectrum, $|\varrho_1|=1$, and the matrix elements $G(\ell,m;z)$ do not decay with the distance $|\ell-m|$.

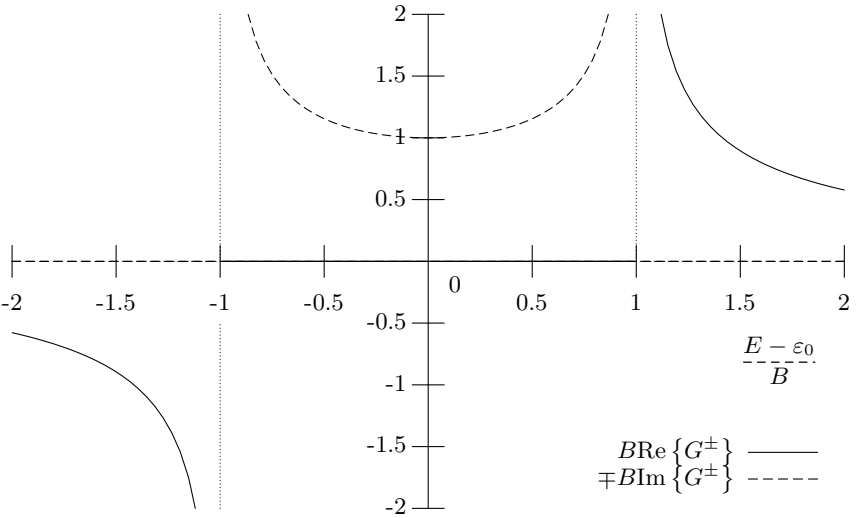

Fig. 5.6. The diagonal matrix element $G^{\pm}(\ell,\ell;E)$ vs. E for the 1-d lattice. $B=2\,|V|$ is half the bandwidth

5.3.2 Square Lattice

For the square lattice we have, by substituting (5.18) into (5.23),

$$G\left(\boldsymbol{\ell},\boldsymbol{m};z\right) = \frac{a^2}{(2\pi)^2}\int_{1\mathrm{BZ}}\mathrm{d}^2k\frac{\mathrm{e}^{\mathrm{i}\boldsymbol{k}\cdot\left(\boldsymbol{\ell}-\boldsymbol{m}\right)}}{z-\varepsilon_0-2V\left[\cos\left(k_1a\right)+\cos\left(k_2a\right)\right]}\,, \tag{5.33}$$

where

$$\boldsymbol{k}\cdot\left(\boldsymbol{\ell}-\boldsymbol{m}\right) = a\left[k_1\left(\ell_1-m_1\right)+k_2\left(\ell_2-m_2\right)\right]\,. \tag{5.34}$$

Here ℓ_1, ℓ_2, m_1, and m_2 are integers, a is the lattice constant; in the present case, the first Brillouin zone is the square

$$-\pi/a \le k_1 < \pi/a \;, \quad -\pi/a \le k_2 < \pi/a \;.$$

Thus (5.33) can be rewritten as

$$\begin{aligned} & G\left(\boldsymbol{\ell}, \boldsymbol{m}; z\right) \\ & = \frac{1}{(2\pi)^2} \int_{-\pi}^{\pi} \mathrm{d}\phi_1 \int_{-\pi}^{\pi} \mathrm{d}\phi_2 \frac{\exp\left[\mathrm{i}\phi_1\left(\ell_1 - m_1\right) + \mathrm{i}\phi_2\left(\ell_2 - m_2\right)\right]}{z - \varepsilon_0 - 2V\left(\cos\phi_1 + \cos\phi_2\right)} \\ & = \frac{1}{\pi^2} \int_0^{\pi} \mathrm{d}\phi_1 \int_0^{\pi} \mathrm{d}\phi_2 \frac{\cos\left[\phi_1\left(\ell_1 - m_1\right)\right] \cos\left[\phi_2\left(\ell_2 - m_2\right)\right]}{z - \varepsilon_0 - 2V\left(\cos\phi_1 + \cos\phi_2\right)} \qquad (5.35a) \\ & = \frac{1}{\pi^2} \int_0^{\pi} \mathrm{d}\phi_1 \int_0^{\pi} \mathrm{d}\phi_2 \left\{ \frac{\cos\left[\left(\ell_1 - m_1 + \ell_2 - m_2\right)\phi_1\right]}{z - \varepsilon_0 - 4V\cos\phi_1\cos\phi_2} \right. \\ & \qquad \left. \times \cos\left[\left(\ell_1 - m_1 - \ell_2 + m_2\right)\phi_2\right] \right\} \;. \qquad (5.35b) \end{aligned}$$

For a derivation of the last expression see [65]. By taking matrix elements of the operator equation, $(z - \mathcal{H})G = 1$, one obtains recurrence relations that allow one to express the arbitrary matrix element $G\left(\boldsymbol{\ell}, \boldsymbol{m}; z\right)$ in terms of the matrix elements $G\left(\boldsymbol{\ell}, \boldsymbol{m}; z\right)$ with $\ell_1 - m_1 = \ell_2 - m_2$ [65] [see also (5.47) below]. Furthermore, the matrix elements $G\left(\boldsymbol{\ell}, \boldsymbol{m}; z\right)$ with $\ell_1 - m_1 = \ell_2 - m_2$ can be expressed by recurrence relations in terms of the diagonal matrix element $G\left(\boldsymbol{\ell}, \boldsymbol{\ell}; z\right)$ and the matrix element $G\left(\boldsymbol{\ell}, \boldsymbol{m}; z\right)$ with $\ell_1 - m_1 = \ell_2 - m_2 = 1$, which will be denoted by $G(1; z)$ [65] (see also Problem 5.3). For the diagonal matrix element $G\left(\boldsymbol{\ell}, \boldsymbol{\ell}; z\right)$ we have

$$\begin{aligned} G\left(\boldsymbol{\ell}, \boldsymbol{\ell}; z\right) &= \frac{1}{2\pi} \int_{-\pi}^{\pi} \mathrm{d}\phi_1 \frac{1}{2\pi} \int_{-\pi}^{\pi} \mathrm{d}\phi_2 \frac{1}{z - \varepsilon_0 + B\cos\phi_1\cos\phi_2} \\ &= \frac{1}{2\pi} \int_{-\pi}^{\pi} \mathrm{d}\phi_1 \frac{1}{\sqrt{\left(z - \varepsilon_0\right)^2 - B^2\cos^2\phi_1}} \\ &= \frac{1}{\pi\left(z - \varepsilon_0\right)} \int_0^{\pi} \frac{\mathrm{d}\phi}{\sqrt{1 - \lambda^2\cos^2\phi}} \;, \qquad (5.36) \end{aligned}$$

where

$$\lambda = \frac{B}{z - \varepsilon_0} \;; \qquad B = 4\left|V\right| \;, \qquad (5.37)$$

hence

$$G\left(\boldsymbol{\ell}, \boldsymbol{\ell}; z\right) = \frac{2}{\pi\left(z - \varepsilon_0\right)} \mathcal{K}(\lambda) \;, \qquad (5.38)$$

where $\mathcal{K}$ is the complete elliptic integral of the first kind. In a similar way, by performing the integration over ϕ_2 we obtain from (5.35b)

$$G(1;z) = \frac{1}{\pi}\int_0^{\pi} \mathrm{d}\phi_1 \frac{\cos(2\phi_1)}{\sqrt{(z-\varepsilon_0)^2 - B^2\cos^2\phi_1}} \tag{5.39a}$$

$$= \frac{2}{\pi(z-\varepsilon_0)}\left[\left(\frac{2}{\lambda^2}-1\right)\mathcal{K}(\lambda) - \frac{2}{\lambda^2}\mathcal{E}(\lambda)\right], \tag{5.39b}$$

where $\mathcal{E}(\lambda)$ is the complete elliptic integral of the second kind.

For $z = E + \mathrm{i}s$, $s \to 0^{\pm}$ and E within the band, one may use the analytic continuation of $\mathcal{K}(\lambda)$ and $\mathcal{E}(\lambda)$ [1] to obtain explicit expressions for $G^{\pm}(\boldsymbol{\ell},\boldsymbol{\ell};E)$ and $G^{\pm}(1;z)$; e.g., for $G^{\pm}(\boldsymbol{\ell},\boldsymbol{\ell};E)$ we have

$$G(\boldsymbol{\ell},\boldsymbol{\ell};E) = \frac{2}{\pi(E-\varepsilon_0)}\mathcal{K}\left(\frac{B}{E-\varepsilon_0}\right), \quad |E-\varepsilon_0| > 4|V| = B,$$

$$\mathrm{Re}\left\{G^{\pm}(\boldsymbol{\ell},\boldsymbol{\ell};E)\right\} = -\frac{2}{\pi B}\mathcal{K}\left(\frac{E-\varepsilon_0}{B}\right), \qquad -B < E-\varepsilon_0 < 0,$$

$$\mathrm{Re}\left\{G^{\pm}(\boldsymbol{\ell},\boldsymbol{\ell};E)\right\} = \frac{2}{\pi B}\mathcal{K}\left(\frac{E-\varepsilon_0}{B}\right), \qquad 0 < E-\varepsilon_0 < B,$$

$$\mathrm{Im}\left\{G^{\pm}(\boldsymbol{\ell},\boldsymbol{\ell};E)\right\} = \mp\frac{2}{\pi B}\mathcal{K}\left(\sqrt{1-\frac{(E-\varepsilon_0)^2}{B^2}}\right), \quad |E-\varepsilon_0| < B\,. \tag{5.40}$$

The density of states per site is given by

$$\varrho(E) = \mp\frac{1}{\pi}\mathrm{Im}\left\{G^{\pm}(\boldsymbol{\ell},\boldsymbol{\ell};E)\right\}$$

$$= \frac{2}{\pi^2 B}\theta(B-|E-\varepsilon_0|)\,\mathcal{K}\left(\sqrt{1-\frac{(E-\varepsilon_0)^2}{B^2}}\right). \tag{5.41}$$

These functions are plotted in Fig. 5.7. Note that the DOS exhibits at both band edges a discontinuity that produces the logarithmic singularities of the $\mathrm{Re}\{G\}$ at the band edges. As was discussed before, this behavior is characteristic of the two-dimensionality of the system. Note also the singularity at the interior of the band (at $E = \varepsilon_0$); the $\mathrm{Re}\{G^{\pm}\}$ is discontinuous there and $\mathrm{Im}\{G^{\pm}\}$ has a logarithmic singularity. The singularities of $G^{\pm}$ within the band are associated with saddle points in the function $E(\boldsymbol{k})$. A minimum number of such saddle points exists and depends on the number of independent variables $k_1,\ldots,k_d$ [66,67] (see Problem 5.8 at the end of this chapter).

As was mentioned before, recurrence relations allow one to express all $G(\boldsymbol{\ell},\boldsymbol{m};z)$ in terms of $G(0;z) \equiv G(\boldsymbol{\ell},\boldsymbol{\ell};z)$, (5.38), and $G(1;z)$, (5.39). These recurrence relations develop numerical instabilities for $|E-\varepsilon_0| \geq B$, especially along the direction of the x- and y-axes. The reason is that the recurrence relations are satisfied not only by the Green's functions, which decay to zero as $|\boldsymbol{\ell}-\boldsymbol{m}| \to \infty$, but by an independent set as well, which blows up as $|\boldsymbol{\ell}-\boldsymbol{m}| \to \infty$. Because of numerical errors, a very small component of this divergent set is present in $G(0;z)$ and $G(1;z)$ and magnified as $|\boldsymbol{\ell}-\boldsymbol{m}|$ increases,

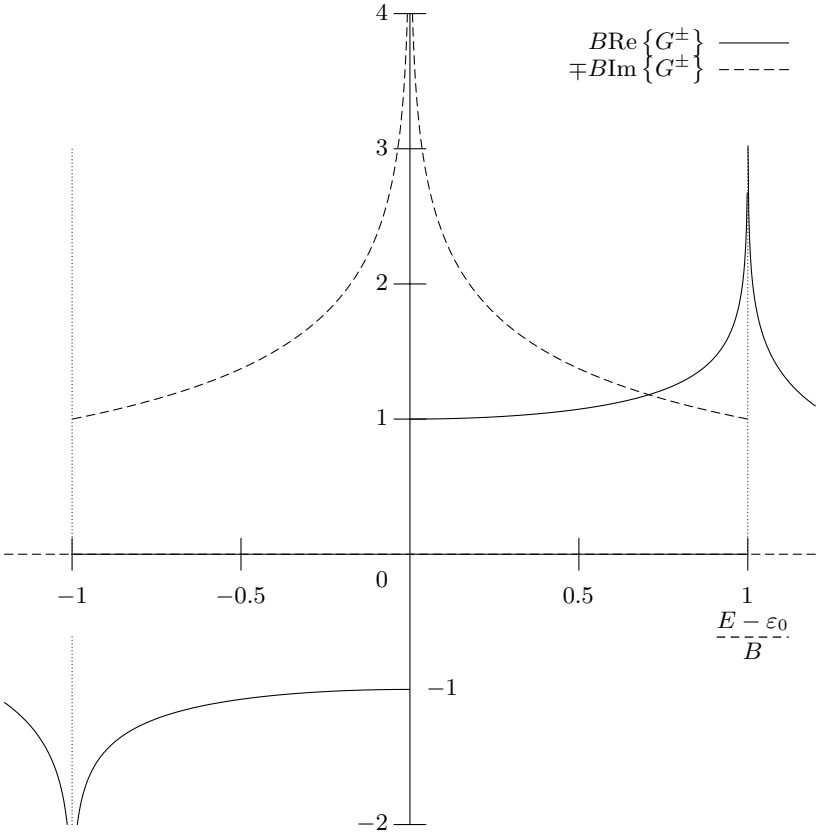

Fig. 5.7. Diagonal matrix elements $G^{\pm}(\boldsymbol{\ell}, \boldsymbol{\ell}; E)$ vs. E for the 2-d square lattice. $B = 4|V|$ is half the bandwidth

until it eventually dominates the solution. To avoid this difficulty, one has to use asymptotic expansions of $G(\boldsymbol{m}, 0; z)$, which are valid for $|\boldsymbol{m}| \gg R_0$ [see (5.42) below] and which can be obtained using the method of stationary phase in evaluating the integral for $G(\boldsymbol{m}, 0; z)$ [68]. See also the solution of Problem 5.2s, equation (15). Setting $\boldsymbol{k}_0 \cdot \boldsymbol{R} = k_{01} a m_1 + k_{02} a m_2 = \phi_{01} m_1 + \phi_{02} m_2$, $R = |m|\, a$, $|m| = \sqrt{m_1^2 + m_2^2}$, and

$$R_0 \equiv \frac{\sqrt{\sin^2 \phi_{01} + \sin^2 \phi_{02}}}{\left| \frac{\varepsilon_0 - E}{2|V|} \left(1 - \cos \phi_{01} \cos \phi_{02}\right) \right|} , \tag{5.42}$$

we find for $|E - \varepsilon_0| < B$ and for $|\boldsymbol{m}| \gg R_0$

$$2\,|V|\, G^{+}(\boldsymbol{m}, 0; E) = \frac{\pm 1 - \mathrm{i}}{2\sqrt{\pi}} \frac{\exp\left[\mathrm{i}\left(m_1 \phi_{01} + m_2 \phi_{02}\right)\right]}{\sqrt{|\boldsymbol{m}|/R_0}} , \tag{5.43}$$

where the upper (lower) sign corresponds to $E > \varepsilon_0$ ($E < \varepsilon_0$), m_1 and m_2 are the cartesian components of $\boldsymbol{m}$, and ϕ_{01} and ϕ_{02} are solutions of the following relations:

$$(\varepsilon_0 - E)/2|V| = \cos\phi_{01} + \cos\phi_{02} \,, \tag{5.44}$$

$$m_2 \sin\phi_{01} = m_1 \sin\phi_{02} \,, \tag{5.45}$$

$$m_1 \sin\phi_{01} \geq 0 \,. \tag{5.46}$$

It follows from (5.42)–(5.46) that the length R_0 (in units of the lattice spacing a) depends on the direction m_1/m_2 as well as the energy E. In particular, as we approach the singular points $E = \varepsilon_0$ and $E = \varepsilon_0 \pm B$, the quantity $R_0 \to \infty$.

In the limit $E \to \varepsilon_0$, $\cos\phi_{01} \to -\cos\phi_{02}$, $\sin^2\phi_{01} \to \sin^2\phi_{02}$, and thus

$$R_0 \to \left|\frac{2V}{E-\varepsilon_0}\right| \frac{\sqrt{2}\,|\sin\phi_{01}|}{1+\cos^2\phi_{01}} \to \infty \quad \text{as} \quad E \to \varepsilon_0 \,. \tag{5.42$'$}$$

R_0 being infinite implies that $G(\boldsymbol{m}, 0; E)$ does not decay as $|\boldsymbol{m}| \to \infty$ when $E = \varepsilon_0$. Indeed, by using the defining equation $(E - \mathcal{H})G = 1$, or more explicitly

$$(E-\varepsilon_0)\, G(\boldsymbol{m}, 0; E) - \sum_{\boldsymbol{\ell} \neq \boldsymbol{m}} \langle \boldsymbol{m} \,|\, \mathcal{H} \,|\, \boldsymbol{\ell} \rangle \langle \boldsymbol{\ell} \,|\, G \,|\, 0 \rangle = \delta_{\boldsymbol{m},0} \,, \tag{5.47}$$

we find in the limit $E = \varepsilon_0$ that

$$G^{\pm}(\boldsymbol{m}, 0; E) = \frac{(-1)^{m_1}}{4V} = \frac{(-1)^{m_1+1}}{4|V|} \,, \qquad m_1 - m_2 = \text{odd} \,,$$

when the difference $m_1 - m_2$ is an odd integer. In the case where $m_1 - m_2$ is an even integer, all $G(\boldsymbol{m}, 0; E)$ blow up as $E \to \varepsilon_0$. We can show that, to the leading order in $E - \varepsilon_0 \to 0$, we have

$$G(\boldsymbol{m}, 0; E) \simeq (-1)^{m_1} G(0, 0; E) \,, \qquad m_1 - m_2 = \text{even.}$$

To prove this last relation, show first that the difference $\delta G(\boldsymbol{m}, 0; E) \equiv G(\boldsymbol{m}, 0; E) - (-1)^{m_1} G(0, 0; E)$ is finite in the limit $E \to \varepsilon_0$; then use the recursion relation (5.47).

In the limit $E \to \varepsilon_0 - B$, the quantity $R_0 \to \sqrt{|V|\,/\,|E - \varepsilon_0 + B|} \to \infty$. Hence $G(\boldsymbol{m}, 0; E)$ does not decay as $E \to \varepsilon_0 - B$ since $R \to \infty$; furthermore, all $G(\boldsymbol{m}, 0; E)$ blow up in the limit $E \to \varepsilon_0 - B$. In the same limit, the differences $\delta G(\boldsymbol{m}, 0; E) \equiv G(\boldsymbol{m}, 0; E) - G(0; E)$ are finite numbers [69] that obey the same recurrence relations as the Gs; the starting values for $\delta G(\boldsymbol{m}, 0; E)$ with $m_1 = m_2$ are $\delta G(0; E) = 0$ and $\delta G(1; E) = -1/(\pi|V|)$. Using these values and the recurrence relations obtained by Morita [65] or by solving Problem 5.3, we obtain first $\delta G(\boldsymbol{m}, 0; E)$ for $m_1 = m_2$ and then, by employing (5.47), we can calculate the Green's function elements for $m_1 \neq m_2$. However, these recurrence relations may eventually develop numerical instabilities.

For E outside the band, the quantities ϕ_1 and ϕ_2 in (5.43) become imaginary, and consequently $G(\boldsymbol{m}, 0; E)$ decays exponentially with the distance $|\boldsymbol{m}|$. In particular, for $E = \varepsilon_0 - B - \delta E$, $\delta E > 0$, and $\delta E/B \ll 1$, one obtains for large $|\boldsymbol{m}|$

$$2\,|V|\,G\left(\boldsymbol{m}, 0; \varepsilon_0 - B - \delta E\right) = -\frac{\exp\left(-|\boldsymbol{m}|\,\sqrt{\delta E/\,|V|}\right)}{\sqrt{2\pi}\left(|\boldsymbol{m}|^2\,\delta E/\,|V|\right)^{1/4}}\,. \tag{5.48}$$

Similar relations appear at the upper band edge $E = \varepsilon_0 + B$. Several other 2-d lattices have been studied. Thus, Horiguchi [70] has expressed Green's functions for the triangular and honeycomb lattices in terms of the complete elliptic integrals of the first and second kind. Horiguchi and Chen [71] obtained the Green's function for the diced lattice. For all these lattices, the DOS exhibits the characteristic discontinuity at the band edges and $\mathrm{Re}\,\{G\}$ has a logarithmic singularity. There are singular points within the band where the $\mathrm{Re}\,\{G\}$ exhibits a discontinuity and the DOS has a logarithmic singularity.

If we are not interested in quantitative details, we can approximate the Green's functions for 2-d lattices by a simple function that retains the correct analytic behavior near the band edges and that gives one state per site. This simple approximation is

$$G(\boldsymbol{\ell}, \boldsymbol{\ell}; z) = \frac{1}{2B}\ln\left(\frac{z - \varepsilon_0 + B}{z - \varepsilon_0 - B}\right)\,, \tag{5.49}$$

which gives the following DOS:

$$\varrho(E) = \frac{1}{2B}\theta\left(B - |E - \varepsilon_0|\right)\,. \tag{5.50}$$

We must stress that the simple expression (5.49) does not correspond to a real 2-d lattice and that it does not possess any Van Hove singularity in the interior of the band. In Fig. 5.8 we plot $G(\boldsymbol{\ell}, \boldsymbol{\ell}; E)$ as given by (5.49) vs. E.

5.3.3 Simple Cubic Lattice

The first Brillouin zone for the simple cubic lattice is the cube

$$-\pi/a \le k_1 < \pi/a\,, \quad -\pi/a \le k_2 < \pi/a\,, \quad -\pi/a \le k_3 < \pi/a\,,$$

where a is the lattice constant. Substituting (5.19) into (5.22) and introducing the variables $\phi_i = k_i a$ $(i = 1, 2, 3)$ we obtain

$$\begin{aligned} G\left(\boldsymbol{\ell}, \boldsymbol{m}; z\right) = {} & \frac{1}{(2\pi)^3}\int_{-\pi}^{\pi}\mathrm{d}\phi_1\int_{-\pi}^{\pi}\mathrm{d}\phi_2\int_{-\pi}^{\pi}\mathrm{d}\phi_3 \\ & \times\frac{\cos\left[\left(\ell_1 - m_1\right)\phi_1 + \left(\ell_2 - m_2\right)\phi_2 + \left(\ell_3 - m_3\right)\phi_3\right]}{z - \varepsilon_0 - 2V\left(\cos\phi_1 + \cos\phi_2 + \cos\phi_3\right)}\,. \end{aligned} \tag{5.51}$$

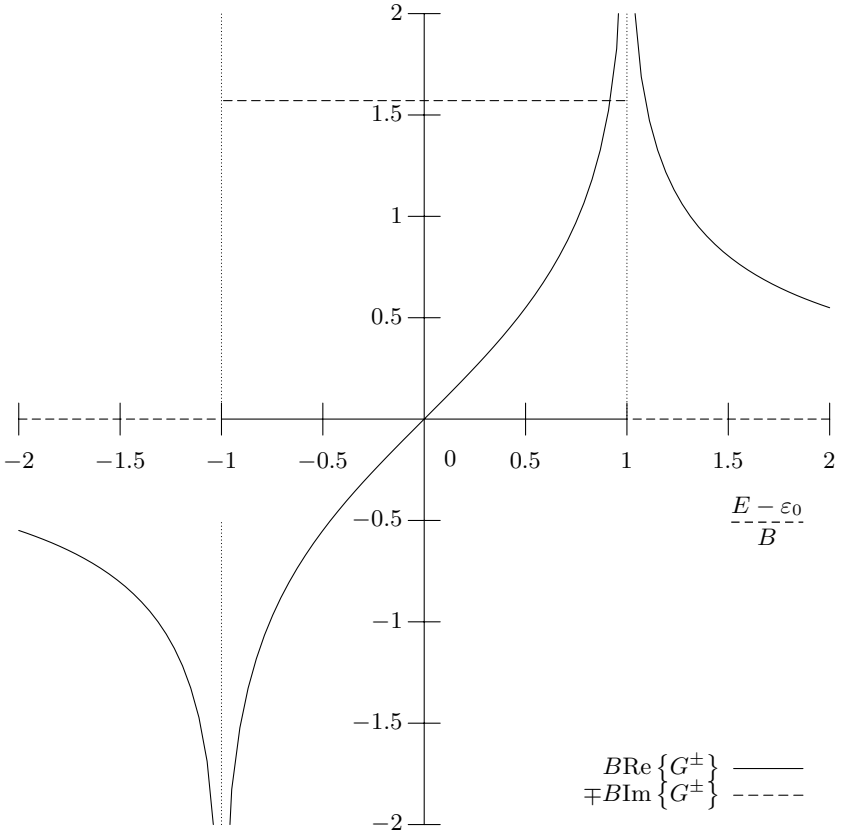

Fig. 5.8. Plot of $\mathrm{Re}\{G^{\pm}\}$ and $\mp\mathrm{Im}\{G^{\pm}\}$ vs. E for approximate expression $G(\boldsymbol{\ell},\boldsymbol{\ell};z) = \ln\left[(z-\varepsilon_0+B)/(z-\varepsilon_0-B)\right]/2B$, where $B = 4|V|$ is half the bandwidth. Compare with the exact expression for the square lattice (Fig. 5.7)

In particular, the diagonal matrix element $G(\boldsymbol{\ell},\boldsymbol{\ell};z)$ is

$$G(\boldsymbol{\ell},\boldsymbol{\ell};z) = \frac{1}{(2\pi)^3}\int_{-\pi}^{\pi}\mathrm{d}\phi_1\int_{-\pi}^{\pi}\mathrm{d}\phi_2\int_{-\pi}^{\pi}\mathrm{d}\phi_3 \times \frac{1}{z-\varepsilon_0-2V(\cos\phi_1+\cos\phi_2+\cos\phi_3)}\,; \tag{5.52}$$

the integration over ϕ_2 and ϕ_3 in (5.52) can be done as in the square lattice case yielding $t\mathcal{K}(t)/2\pi V$, where

$$t = \frac{4V}{z-\varepsilon_0-2V\cos\phi_1}\,; \tag{5.53}$$

thus

$$G(\boldsymbol{\ell}, \boldsymbol{\ell}; z) = \frac{1}{2\pi^2 V} \int_0^\pi \mathrm{d}\phi_1 t\mathcal{K}(t) \; . \tag{5.54}$$

The last integral can be calculated numerically [72]. $\mathrm{Re}\{G^{\pm}(\boldsymbol{\ell}, \boldsymbol{\ell}; E)\}$ and $\mp\mathrm{Im}\{G^{\pm}(\boldsymbol{\ell}, \boldsymbol{\ell}; E)\}$ for real E are plotted in Fig. 5.9. The behavior is typical for a 3-d system: near both band edges, the DOS, $-\mathrm{Im}\{G^{+}\}/\pi$, approaches zero continuously as $\sqrt{|\Delta E|}$, where $|\Delta E|$ is the difference of E and the corresponding band edge. $\mathrm{Re}\{G\}$ remains finite around the band edges, although its derivative with respect to E blows up as we approach the band edges from outside the band. Within the band are two Van Hove singularities, where both $\mathrm{Im}\{G\}$ and $\mathrm{Re}\{G\}$ are continuous while their derivatives are discontinuous and blow up sidewise (however, see point 4 in Problem 5.8).

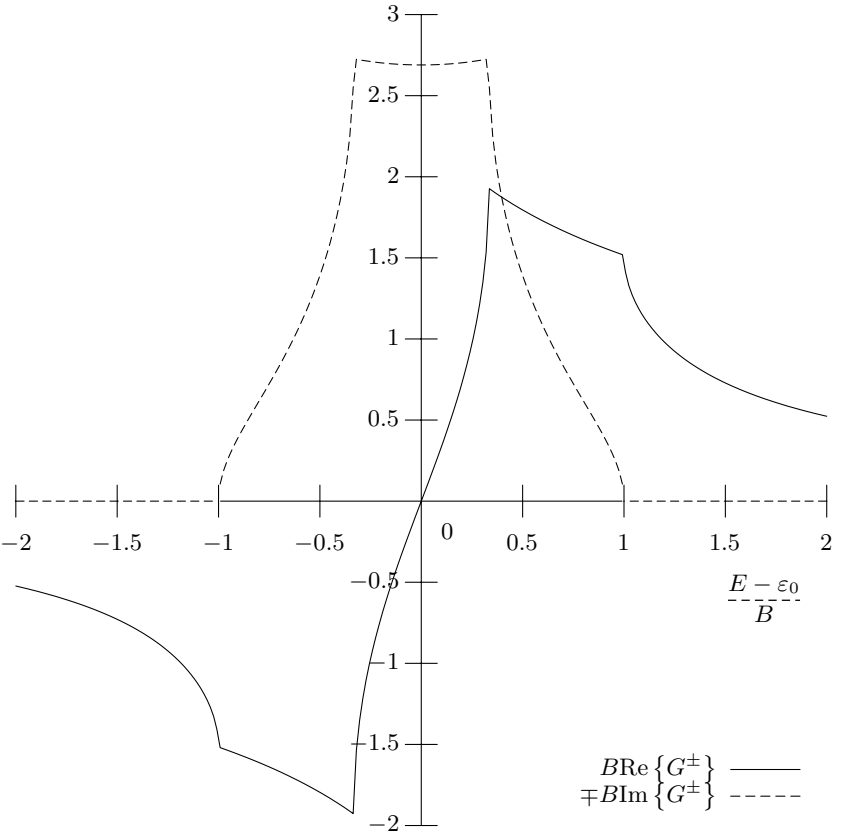

Fig. 5.9. Diagonal matrix elements $G(\boldsymbol{\ell}, \boldsymbol{\ell}; E)$ vs. E for simple cubic lattice. $B = 6|V|$ is half the bandwidth

When $|\boldsymbol{\ell} - \boldsymbol{m}|$ is along an axis (e.g., the x-axis), one can perform the integration over ϕ_2 and ϕ_3 in (5.51) as in the square lattice, yielding again $t\mathcal{K}(t)/2\pi V$; thus

$$G(\ell_1 - m_1, 0, 0; z) = \frac{1}{2\pi^2 V} \int_0^\pi \mathrm{d}\phi_1 \cos\left[(\ell_1 - m_1)\,\phi_1\right] t\mathcal{K}(t) \; . \tag{5.55}$$

Details concerning the evaluation of integral (5.55) are given in [73]; in the same reference some recurrence relations[1] are obtained that allow the computation of $G(\boldsymbol{\ell}, \boldsymbol{m}; z)$ for small $|\boldsymbol{\ell} - \boldsymbol{m}|$ in terms of $G(\ell_1 - m_1, 0, 0; z)$. Using these techniques, Table 5.2 at the end of this chapter was constructed. Joyce [74] was able to prove that $G(\boldsymbol{\ell}, \boldsymbol{\ell}; z)$ can be expressed as a product of two complete elliptic integrals of the first kind. Morita [75] obtained recurrence relations for the simple cubic lattice that allow the evaluation of all $G(\boldsymbol{\ell}, \boldsymbol{m})$ in terms of $G(0,0,0) \equiv G(\boldsymbol{\ell}, \boldsymbol{\ell})$, $G(2,0,0)$, and $G(3,0,0)$. The last two Green's functions were expressed by Horiguchi and Morita [76] in closed forms in terms of complete elliptic integrals. The reader is also referred to the papers by Austen and Loly [77], by Hioe [78], by Rashid [79], by Inawashiro et al. [80], by Katsura et al. [81], and by Joyce [82]. Asymptotic expansions valid for large values of $|\boldsymbol{\ell} - \boldsymbol{m}|$ were obtained [68]; within the band $G(\boldsymbol{\ell}, \boldsymbol{m})$ decays slowly as $|\boldsymbol{\ell} - \boldsymbol{m}|^{-1}$; outside the band it decays exponentially (Problem 5.4.)

The Green's functions for other 3-d lattices, such as face- and body-centered cubic, have been calculated [72, 75, 77–79, 83–88]. Note that the Green's functions for the fcc and bcc lattices blow up at the upper band edge and in the interior of the band, respectively [72] (Problem 5.5s). This behavior is atypical for a 3-d system. A small perturbation such as the inclusion of second-nearest-neighbor transfer matrix elements will eliminate these pathological infinities.

In many cases where quantitative details are not important, it is very useful to have a simple approximate expression (for G) that can be considered as typical for a 3-d lattice. Such an expression must exhibit the correct analytic behavior near the band edges and must give one state per site. Such a simple expression, widely used and known as the Hubbard Green's function, is the following:

$$G(\boldsymbol{\ell}, \boldsymbol{\ell}; z) = \frac{2}{z - \varepsilon_0 + \sqrt{(z - \varepsilon_0)^2 - B^2}} \; , \tag{5.56}$$

where the sign of $\mathrm{Im}\left\{\sqrt{(z - \varepsilon_0)^2 - B^2}\right\}$ is the same as the sign of $\mathrm{Im}\{z\}$. The DOS corresponding to (5.56) is of a semicircular form: the real and imaginary parts of G as given by (5.56) are shown in Fig. 5.10. Note that the simple approximation (5.56) does not reproduce any Van Hove singularity within the band.

[1] There is a typographical error in (3.8) and (3.9) of [73]: $G_{sc}(t; 1, 0, 0)$ must be multiplied by t^3 instead of t^2.

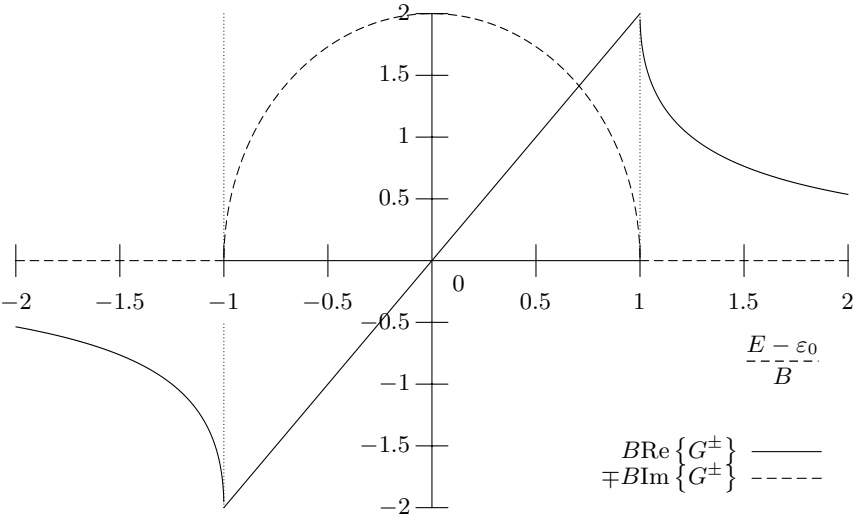

Fig. 5.10. $\mathrm{Re}\{G^{\pm}\}$ and $\mp\mathrm{Im}\{G^{\pm}\}$ vs. E for approximate 3-d $G(\boldsymbol{\ell},\boldsymbol{\ell};z) = 2\Big/\left[(z-\varepsilon_0)+\sqrt{(z-\varepsilon_0)^2-B^2}\right]$, where B is half the bandwidth. Compare with the exact $G(\boldsymbol{\ell},\boldsymbol{\ell};z)$ for the simple cubic lattice (Fig. 5.9)

5.3.4 Green's Functions for Bethe Lattices (Cayley Trees)

Bethe lattices or Cayley trees are lattices which have no closed loops and are completely characterized by the number of nearest neighbors Z or the connectivity $K = Z - 1$. In Fig. 5.11 we show a portion of a Bethe lattice for $K = 2$ ($Z = 3$). The 1-d lattice is a Cayley tree with $K = 1$ ($Z = 2$).

Calculation of Green's functions in Bethe lattices can be performed by using the renormalized perturbation expansion (RPE) as explained in Appendix F.

For the double spacing periodic case shown in Fig. 5.11 (with $\varepsilon_1 > \varepsilon_2$), the result for $G(\ell,\ell;z)$ is (Appendix F)

$$G(\ell,\ell;z) = G_1(z) \equiv \frac{2K(z-\varepsilon_2)}{D}\,; \qquad \varepsilon_\ell = \varepsilon_1\,,$$
$$G_2(z) \equiv \frac{2K(z-\varepsilon_1)}{D}\,; \qquad \varepsilon_\ell = \varepsilon_2\,. \tag{5.57}$$

Here D is given by

$$D = (K-1)(z-\varepsilon_1)(z-\varepsilon_2) + (K+1)\sqrt{(z-\varepsilon_1)(z-\varepsilon_2)\left[(z-\varepsilon_1)(z-\varepsilon_2)-4KV^2\right]}\,, \tag{5.58}$$

where the sign of the imaginary part of the square root in (5.58) is the same as the sign of $\mathrm{Im}\{(z-\varepsilon_1)(z-\varepsilon_2)\}$. For the off-diagonal matrix element

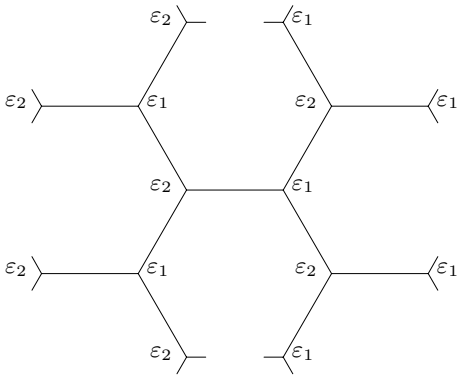

Fig. 5.11. Part of a Bethe lattice (Cayley tree) with $Z = 3$ nearest neighbors. The site energies $\{\varepsilon_\ell\}$ are arranged in an alternating periodic manner

$G(\ell, m; z)$ we have (Appendix F)

$$G(\ell, m) = G(\ell, \ell)V^{|m-\ell|}[G(\ell+1, \ell+1[\ell])]^{|m-\ell|/2} \times [G(\ell, \ell[\ell+1])]^{|m-\ell|/2} , \tag{5.59a}$$

when $|m - \ell|$ even,

$$G(\ell, m) = G(\ell, \ell)V^{|m-\ell|}[G(\ell+1, \ell+1[\ell])]^{(|m-\ell|+1)/2} \times [G(\ell, \ell[\ell+1])]^{(|m-\ell|-1)/2} ; \tag{5.59b}$$

when $|m - \ell|$ odd, and

$$G\left(\ell+1, \ell+1[\ell]; z\right) = \frac{K+1}{z - \varepsilon_{\ell+1} + K\left[G(\ell+1, \ell+1; z)\right]^{-1}} , \tag{5.60}$$

$$G\left(\ell, \ell[\ell+1]; z\right) = \frac{K+1}{z - \varepsilon_\ell + K\left[G(\ell, \ell; z)\right]^{-1}} . \tag{5.61}$$

As can be seen from (5.58), the spectrum consists of two subbands, the lower one extending from $(\varepsilon_1 + \varepsilon_2)/2 - \sqrt{(\varepsilon_1 - \varepsilon_2)^2/4 + 4KV^2}$ to ε_2 and the upper one from ε_1 to $(\varepsilon_1 + \varepsilon_2)/2 + \sqrt{(\varepsilon_1 - \varepsilon_2)^2/4 + 4KV^2}$. There is a gap from ε_2 to ε_1. The DOS at sites with $\varepsilon_1(\varepsilon_2)$ is $\varrho_1\,(\varrho_2)$, where

$$\varrho_i(E) = -\frac{1}{\pi}\mathrm{Im}\left\{G_i^+(E)\right\} \;; \quad i = 1, 2 . \tag{5.62}$$

A plot of $G_1(z)$ is shown in Fig. 5.12. Note the analytic behavior at the band edges, which is typical 3-d except at one of the interior band edges, where a square root divergence appears.

The double spacing periodic case in a Cayley tree describes the basic qualitative features of ionic crystals such as NaCl and CsCl. Indeed, in these materials, the lower subband is fully occupied by electrons while the upper subband

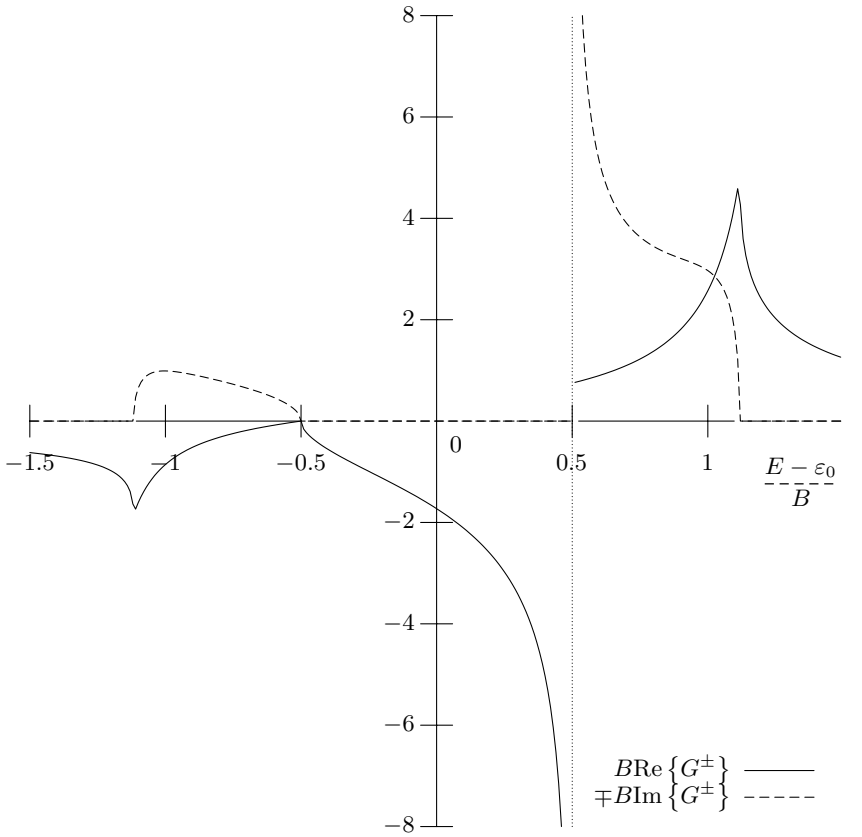

Fig. 5.12. $\mathrm{Re}\{G^{\pm}(\ell,\ell)\}$ and $\mp\mathrm{Im}\{G^{\pm}(\ell,\ell)\}$ vs. E for a Bethe lattice with four nearest neighbors ($K=3$); $\varepsilon_{\ell+2n}=\varepsilon_1$, $\varepsilon_{\ell+2n+1}=\varepsilon_2$, where n integer and $\varepsilon_1\geq\varepsilon_2$; $\varepsilon_0=(\varepsilon_1+\varepsilon_2)/2$, $B=2\sqrt{K\bar{V}^2}$ and the difference $\varepsilon_1-\varepsilon_2$ has been taken equal to B. $\mathrm{Re}\{G^{\pm}(\ell+1,\ell+1;E)\}=-\mathrm{Re}\{G^{\pm}(\ell,\ell;-E+2\varepsilon_0)\}$; $\mathrm{Im}\{G^{\pm}(\ell+1,\ell+1;E)\}=\mathrm{Im}\{G^{\pm}(\ell,\ell;-E+2\varepsilon_0)\}$

is completely empty. Any electronic excitation has to overcome the gap width, E_g, in order to take place. Thus E_g plays an important role in optical absorption, photoconductivity, electronic polarizability, lattice vibrations, etc. Our simple model gives E_g as being equal to $\varepsilon_1-\varepsilon_2$. If we make the approximation that ε_1 and ε_2 are equal to the corresponding atomic levels, we find $E_g=14.52\,\mathrm{eV}$ for LiF (the experimental value is 13.6 eV), $E_g=8.83\,\mathrm{eV}$ for NaCl (the experimental value is 8.5 eV), and $E_g=7.6\,\mathrm{eV}$ for CsI (the experimental value is 6.2 eV). The subband widths, W, in the large-gap case, where $E_g\gg 4\sqrt{K}\,|V|$, are given by $W\simeq 4KV^2/E_g=B^2/E_g$, where $B\equiv 2\sqrt{K\bar{V}^2}$ is half the bandwidth in the case where $\varepsilon_1=\varepsilon_2$. (In Fig. 5.12 we have taken $\varepsilon_1=-\varepsilon_2=B/2$ so that $E_g=B$ and the width of the subbands is $0.618B$.)

The simple periodic case is obtained by setting $\varepsilon_1 = \varepsilon_2 = \varepsilon_0$. We then have

$$G(\ell, \ell; z) = \frac{2K}{(K-1)(z-\varepsilon_0) + (K+1)\sqrt{(z-\varepsilon_0)^2 - 4KV^2}} , \tag{5.63}$$

where the sign of the imaginary part of the square root is the same as the sign of $\mathrm{Im}\{z\}$. We obtain thus a single band centered around ε_0 with a half bandwidth $B = 2|V|\sqrt{K}$. Note that (5.63) reduces to the Hubbard Green's function in the limit $K \to \infty$ with $B = 2|V|\sqrt{K}$ remaining constant. For the quantity $G(\ell, \ell[\ell+1])$ we have when $\varepsilon_1 = \varepsilon_2 = \varepsilon_0$:

$$G(\ell, \ell[\ell+1]) = \frac{2}{(z-\varepsilon_0) + \sqrt{(z-\varepsilon_0)^2 - 4KV^2}} . \tag{5.64}$$

Hence the off-diagonal matrix elements are

$$G(\ell, m) = \frac{2K}{(K-1)(z-\varepsilon_0) + (K+1)\sqrt{(z-\varepsilon_0)^2 - 4KV^2}} \times \left[\frac{2V}{(z-\varepsilon_0) + \sqrt{(z-\varepsilon_0)^2 - 4KV^2}}\right]^{|\ell-m|} . \tag{5.65}$$

For $K = 1$ the Bethe lattice is identical to the 1-d lattice, and consequently (5.65) reduces to (5.30) when $K = 1$. Similarly, (5.57), (5.59a), and (5.59b) give the double spacing periodic 1-d results when $K = 1$.

Note that the Green's functions for Bethe lattices have several applications in solid-state physics, especially for analyzing amorphous solids [89–92] by the method of "cluster–Bethe–lattice." For a review the reader is referred to a paper by Thorpe [93].

5.4 Summary

In this chapter we introduced the tight-binding Hamiltonian (TBH)

$$\mathcal{H} = \sum_{\boldsymbol{\ell}} |\boldsymbol{\ell}\rangle\, \varepsilon_{\boldsymbol{\ell}}\, \langle \ell| + \sum_{\boldsymbol{\ell m}} |\boldsymbol{\ell}\rangle\, V_{\boldsymbol{\ell m}}\, \langle \boldsymbol{m}| , \qquad V_{\boldsymbol{\ell\ell}} = 0 , \tag{5.7}$$

where each state $|\boldsymbol{\ell}\rangle$ is an atomiclike orbital centered at site $\boldsymbol{\ell}$ and $\langle \boldsymbol{\ell} \,|\, \boldsymbol{n}\rangle = \boldsymbol{\delta_{\ell n}}$. The $\{\boldsymbol{\ell}\}$ sites form a regular lattice. The quantity $\varepsilon_{\boldsymbol{\ell}}$ is the energy of an electron located at site $\boldsymbol{\ell}$ in the absence of $V_{\boldsymbol{\ell m}}$. The quantity $V_{\boldsymbol{\ell m}}$ is the matrix element for transferring an electron from site $\boldsymbol{\ell}$ to site $\boldsymbol{m}$. The electronic motion governed by the TBH (5.7) is mathematically equivalent to the motion of a coupled set of 1-d pendula (Table 5.1).

We examined the case of a periodic TBH with the same period as the lattice. This periodicity implies that

$$\varepsilon_{\boldsymbol{\ell}} = \varepsilon_0 \qquad \text{for all } \boldsymbol{\ell}\,, \tag{5.6a}$$

$$V_{\boldsymbol{\ell m}} = V_{\boldsymbol{\ell}-\boldsymbol{m}}\,. \tag{5.6b}$$

The eigenfunctions and eigenvalues of the periodic TBH are of the following form:

$$|\boldsymbol{k}) = \frac{1}{\sqrt{N}} \sum_{\boldsymbol{i}} \mathrm{e}^{\mathrm{i}\boldsymbol{k}\cdot\boldsymbol{i}}\, |\boldsymbol{i}\rangle\ , \tag{5.15a}$$

$$E\,(\boldsymbol{k}) = \varepsilon_0 + \sum_{\boldsymbol{\ell}} V_{0\boldsymbol{\ell}} \mathrm{e}^{\mathrm{i}\boldsymbol{k}\cdot\boldsymbol{\ell}}\,, \tag{5.15b}$$

where $\boldsymbol{k}$ is restricted to a finite region called the first Brillouin zone. Using the general formula $G(z) = \sum_{\boldsymbol{k}} (|\boldsymbol{k})\,(\boldsymbol{k}|)\,/\,[z - E(\boldsymbol{k})]$ together with (5.15a) and (5.15b), we can calculate $G(z)$. In the case where

$$V_{\boldsymbol{\ell m}} = \begin{cases} V, & \boldsymbol{\ell}, \boldsymbol{m} \text{ nearest neighbors}\,, \\ 0, & \text{otherwise}\,, \end{cases} \tag{5.9a, 5.9b}$$

we obtain explicit expressions for $G(z)$ for various lattices such as the 1-d lattice, the 2-d square, the 3-d simple cubic, and the Bethe lattice (Figs. 5.6, 5.7, 5.9, and 5.12). The analytic behavior of these Green's functions near the band edges depends in general on the dimensionality as in the free-particle case (although exceptions do exist; see Problem 5.5s).

Finally, we discussed briefly the applications of the TBH [or the linear combination of atomic orbitals (LCAO) method] to the problem of the electronic structure of solids.

Further Reading

Several textbooks present the subject of solid-state physics at the introductory level, such as those by Kittel [22] and Ibach and Lüth [23], and to a more advanced level such as the books by Ashcroft and Mermin [28], Marder [30], and Harrison [25].

Problems

5.1s. Prove that $|\varrho_2| > |\varrho_1|$ unless $-1 \le x \le 1$, where ϱ_1 and ϱ_2 are given by (5.29).

5.2s. Using (5.43)–(5.46) prove (5.42).

5.3. Define the functions

$$F_n\left(k^2\right) \equiv \int_0^\pi \mathrm{d}x \frac{\cos(nx)}{\sqrt{1-k^2\cos^2 x}} \,, \tag{1}$$

$$G_n\left(k^2\right) \equiv \int_0^\pi \mathrm{d}x \cos(nx)\sqrt{1-k^2\cos^2 x} \,. \tag{2}$$

Show that

$$G_n\left(k^2\right) = -\frac{k^2}{4}F_{n+2}\left(k^2\right) + \left(1-\frac{k^2}{2}\right)F_n\left(k^2\right) - \frac{k^2}{4}F_{n-2}\left(k^2\right) \,. \tag{3}$$

Show also by partial integration of (2) that

$$G_n\left(k^2\right) = -\frac{k^2}{4n}\left[F_{n-2}\left(k^2\right) - F_{n+2}\left(k^2\right)\right] \,. \tag{4}$$

Comparing (3) and (4) obtain a recurrence relation of F_{n+2} in terms of F_n and F_{n-2}. Use this recurrence relation to obtain a recurrence relation for $G\left(\boldsymbol{m}, 0; E\right)$ when $m_1 = m_2$.

5.4. Following the procedures of Problem 5.2s, prove that the asymptotic expansion of (5.51) for large values of $|\boldsymbol{\ell} - \boldsymbol{m}|$ are given by

$$G\left(\boldsymbol{R}\right) = \frac{-1}{4\pi\left|V\right|}\frac{\exp\left(\mathrm{i}\boldsymbol{k}_0\cdot\boldsymbol{R}\right)}{(R/a)} \times\sqrt{\frac{\sin^2\phi_1+\sin^2\phi_2+\sin^2\phi_3}{\sin^2\phi_1\cos\phi_2\cos\phi_3+\sin^2\phi_2\cos\phi_3\cos\phi_1+\sin^2\phi_3\cos\phi_1\cos\phi_2}} \,.$$

5.5s. Find the E vs. $\boldsymbol{k}$ for the body-centered cubic (bcc) and the face-centered cubic (fcc) lattices within the framework of the Hamiltonian (5.7). Then determine the energies where the DOS blows up.

5.6. To describe qualitatively elemental semiconductors we can consider the simplest possible model, i.e., a 1-d TBM with two atomiclike orbitals per site (one s and one p along the direction of the chain). For the diagonal matrix elements of the Hamiltonian we shall choose the values appropriate for Si ($\varepsilon_s = -14.79\,\mathrm{eV}$ and $\varepsilon_p = -7.58\,\mathrm{eV}$). For the off-diagonal matrix elements we shall make the following choices (see [25]):

$$\begin{aligned}
\langle n,s\,|\,\mathcal{H}\,|\,n+1,s\rangle &= V_2 = -1.32\frac{\hbar^2}{md^2} = -1.32\frac{7.61}{d^2}\,\mathrm{eV} \overset{\text{Si}}{=} -1.82\,\mathrm{eV}\,,\\
\langle n,p\,|\,\mathcal{H}\,|\,n+1,p\rangle &= V_2' = 2.22\frac{\hbar^2}{md^2} = 2.22\frac{7.61}{d^2}\,\mathrm{eV} \overset{\text{Si}}{=} 3.06\,\mathrm{eV}\,,\\
\langle n,s\,|\,\mathcal{H}\,|\,n+1,p\rangle &= -\langle n,p\,|\,\mathcal{H}\,|\,n+1,s\rangle\\
&= V_2'' = 1.42\frac{\hbar^2}{md^2} = 1.42\frac{7.61}{d^2}\,\mathrm{eV} \overset{\text{Si}}{=} 1.96\,\mathrm{eV}\,,
\end{aligned} \tag{1}$$

where d is the bond length (in the last expressions d is in Å). For Si $d = 2.35$ Å.

Show that:

1. For each k there are now two solutions, $E(k)$, given by setting the determinant D equal to zero:

$$D \equiv \begin{vmatrix} E - \varepsilon_s - 2V_2 \cos(kd) & -2\mathrm{i}V_2'' \sin(kd) \\ 2\mathrm{i}V_2'' \sin(kd) & E - \varepsilon_p - 2V_2' \cos(kd) \end{vmatrix} = 0 \,. \tag{2}$$

2. For d very large, two bands are formed around ε_s and ε_p of widths $4\,|V_2|$ and $4V_2'$, respectively. The gap is $E_g = \varepsilon_p - \varepsilon_s - 2\,(V_2' + |V_2|)$.
3. For $d = d_{\mathrm{Si}}$, two bands are formed around $\varepsilon_h - |V_{2h}|$ and $\varepsilon_h + |V_{2h}|$ of width $\varepsilon_p - \varepsilon_s \pm 1.8\hbar^2/md^2$ for the upper and lower band, respectively, where $\varepsilon_h = (\varepsilon_s + \varepsilon_p)/2$, $V_{2h} = -\frac{1}{2}\,(|V_2| + V_2' + 2V_2'')$. So the gap is approximately equal to $2\,|V_{2h}| - (\varepsilon_p - \varepsilon_s)$. Substituting the values for Si we find $E_g \simeq 1.59\,\mathrm{eV}$, to be compared with the experimental value of $E_g = 1.16\,\mathrm{eV}$.
4. Interpret the results in item 3 above by changing the basis from $|s\rangle$ and $|p\rangle$ to the atomic hybrids $|\chi_1\rangle = \frac{1}{\sqrt{2}}\,(|s\rangle + |p\rangle)$ and $|\chi_2\rangle = \frac{1}{\sqrt{2}}\,(|s\rangle - |p\rangle)$ and then to the bonding, $|\psi_{bn}\rangle \equiv \frac{1}{\sqrt{2}}\,(|\chi_{1,n}\rangle + |\chi_{2,n+1}\rangle)$, and the antibonding, $|\psi_{an}\rangle \equiv \frac{1}{\sqrt{2}}\,(|\chi_{1,n}\rangle - |\chi_{2,n+1}\rangle)$, orbitals. By appropriate approximation, the two sets $\{|\psi_{bn}\rangle\}$ and $\{|\psi_{an}\rangle\}$ are decoupled.
5. Plot the four band edges of the two bands as a function of d ($2\text{Å} < d < \infty$) by employing the solutions of (2). Are there values of d where the gap disappears?

5.7s. Starting from (F.10)–(F.13) prove (5.60) and (5.61).

5.8. The states of a quantum particle moving in a periodic potential are characterized by the crystal wavevector $\boldsymbol{k}$ and the band index n. In what follows we shall not display explicitly the band index. (In the TBM we considered in this chapter there is only one band).

Prove that the density of states (DOS) exhibits a singularity, as shown in Fig. 5.13, near an energy E_0 such that $\nabla_{\boldsymbol{k}} E(\boldsymbol{k}) = 0$ for an *isolated* point, $\boldsymbol{k} = \boldsymbol{k}_0$, satisfying the relation $E_0 = E(\boldsymbol{k}_0)$.

The quantities A_i are defined by the relations $A_i \equiv \partial^2 E(\boldsymbol{k})/\partial k_i^2$ for $\boldsymbol{k} = \boldsymbol{k}_0$; the components i are along the principal axes, which by definition satisfy the relations $\partial^2 E(\boldsymbol{k})/\partial k_i \partial k_j = 0$ for $i \neq j$.

Hints:

1. It is better and easier to work first with the quantity $R(E, E_0)$ representing the number of states whose eigenenergies fall between E and E_0. Then the DOS is obtained by taking the derivative

$$\varrho(E) = \frac{\mathrm{d}R(E, E_0)}{\mathrm{d}E} \qquad \text{as } E \to E_0 \,. \tag{1}$$

The number of states, $R(E, E_0)$, per primitive cell (and per band) is given by the general formula

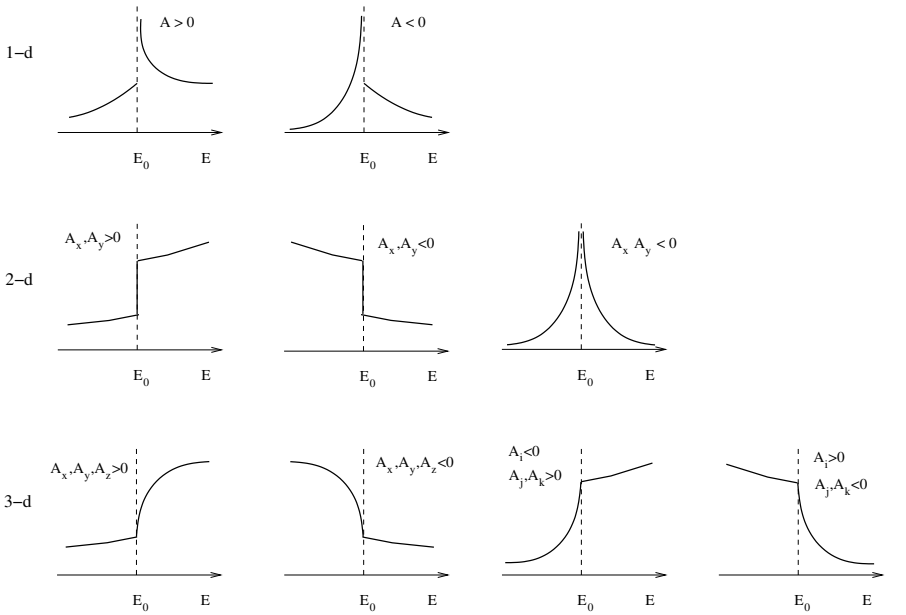

Fig. 5.13. Behavior of DOS near an isolated energy E_0 corresponding to an extremum or a saddle point of $E(\boldsymbol{k})$ for 1-d, 2-d, and 3-d systems

$$R\left(E, E_0\right) = \frac{\Omega_0}{(2\pi)^d} \Omega_{\boldsymbol{k}} \ , \tag{2}$$

where d is the dimensionality of space (d=1,2,3), Ω_0 the "volume" of the primitive cell (a, a^2, a^3 for $d = 1, 2, 3$ and for the examples we have considered), and $\Omega_{\boldsymbol{k}}$ the extent (volume, area, length for $d = 3, 2, 1$, respectively) of the region in $\boldsymbol{k}$-space whose points satisfy the inequalities $E_0 < E\left(\boldsymbol{k}\right) < E$. Notice that the total number of states in the whole first Brillouin zone is exactly one (per band).

2. Consider the $E(k)$ vs. k in the 1-d case as shown schematically in the figure below. When E is below the local minimum E_m, there is only one k point such that $E = E(k)$, and consequently $R(E + \delta E, E) \equiv \varrho(E)\delta E$ is, according to (2), $(a/2\pi)\delta k$. Thus

$$\varrho(E) = \frac{a}{2\pi} \frac{1}{|\mathrm{d}E/\mathrm{d}k|} \ , \qquad E < E_m \ , \tag{3}$$

where the derivative is computed at point k such that $E(k) = E$. If E is between E_m and E_M, then there are three k points such that $E\left(k_i\right) = E$ and the DOS is equal to $(a/2\pi) \sum_{i=1}^{3} |\mathrm{d}E/\mathrm{d}k|_i^{-1}$. For E higher but close to E_m, $R\left(E, E_m\right) = (a/2\pi)\left[k_1 + k_3 - k_2\right]$. But around k_m we can write

$$E = E_m + \frac{1}{2} A \left(k_i - k_m\right)^2 \ , \quad i = 2, 3, \qquad E \to E_m^+ \ . \tag{4}$$

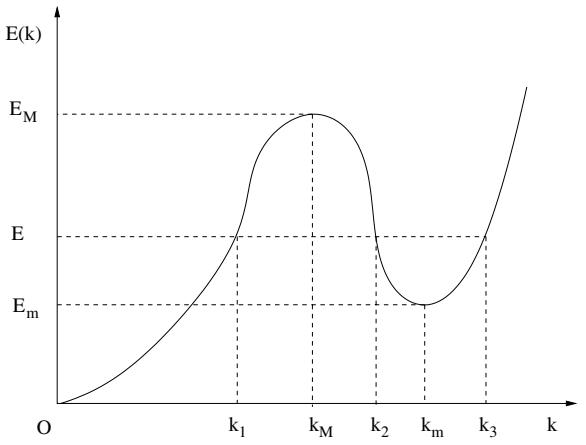

Fig. 5.14. Example of E vs. k for 1-d system

Thus $k_3 - k_m = k_m - k_2 = \sqrt{2\,(E - E_m)\,/A}$. Substituting in $R\,(E, E_m)$ and differentiating with respect to E we find

$$\varrho(E) = \begin{cases} \dfrac{a}{2\pi}\left(\dfrac{1}{|\mathrm{d}E/\mathrm{d}k|_1} + \sqrt{\dfrac{2}{A}}\dfrac{1}{\sqrt{E - E_m}}\right) , & E \to E_m^+ \ , \\ \dfrac{a}{2\pi}\dfrac{1}{|\mathrm{d}E/\mathrm{d}k|_1} , & E \to E_m^- \ . \end{cases} \tag{5}$$

In a similar way show that

$$\varrho(E) = \begin{cases} \dfrac{a}{2\pi}\dfrac{1}{|\mathrm{d}E/\mathrm{d}k|_3} , & E \to E_M^+ \ , \\ \dfrac{a}{2\pi}\left(\dfrac{1}{|\mathrm{d}E/\mathrm{d}k|_3} + \sqrt{\dfrac{2}{A\,(E - E_M)}}\right) , & E \to E_M^- \ . \end{cases} \tag{6}$$

3. In two dimensions we have for E close to E_0, such that $E\,(\boldsymbol{k}_0) = E_0$, and $\nabla_k E(\boldsymbol{k}) = 0$ for $\boldsymbol{k} = \boldsymbol{k}_0$, where $\boldsymbol{k}_0$ is an isolated point:

$$E = E\,(\boldsymbol{k}) = E_0 + \frac{1}{2}A_x\,(k_x - k_{x0})^2 + \frac{1}{2}A_y\,(k_y - k_{y0})^2 \ , \tag{7}$$

where x and y are the principal axes.
If both $A_x > 0$ and $A_y > 0$, then $\boldsymbol{k}_0$ corresponds to a local minimum; if both $A_x < 0$ and $A_y < 0$, then $\boldsymbol{k}_0$ corresponds to a local maximum; finally, if $A_x A_y < 0$, then $\boldsymbol{k}_0$ is a saddle point.
Show that:
(a) If $A_x, A_y > 0$, then for E just above E_0 an extra $\delta R(E, E_0)$ is added corresponding to an ellipse in $\boldsymbol{k}$-space of area proportional to $\delta E = E - E_0$. Thus a discontinuity in the DOS would result in the form

$$\varrho\left(E_0^+\right) - \varrho\left(E_0^-\right) = \frac{a^2}{2\pi}\frac{1}{\sqrt{A_x A_y}} \,. \tag{8}$$

(b) If $A_x, A_y < 0$, then we find a similar expression

$$\varrho\left(E_0^+\right) - \varrho\left(E_0^-\right) = -\frac{a^2}{2\pi}\frac{1}{\sqrt{A_x A_x}} \,. \tag{9}$$

(c) If $A_x A_y < 0$, then the area in $\boldsymbol{k}$ space corresponding to $R\left(\pm E \mp E_0\right)$ is between the two straight lines $k_y - k_{0y} = \pm\sqrt{-A_x/A_y}\left(k_x - k_{x0}\right)$ and the hyperbola $2\left(E - E_0\right) = A_x\left(k_x - k_{x0}\right)^2 + A_y\left(k_y - k_{y0}\right)^2$, where $E - E_0$ is either positive or negative. The corresponding area in $\boldsymbol{k}$-space is

$$\Omega_{\boldsymbol{k}} = \frac{2}{\sqrt{-A_x A_y}}\left|E - E_0\right|\left|\ln\left|E - E_0\right|\right| + O\left(\left|E - E_0\right|\right) \,.$$

Hence

$$\varrho(E) = \frac{a^2}{(2\pi)^2}\frac{2}{\sqrt{-A_x A_y}}\left|\ln\left|E - E_0\right|\right| \qquad \text{as} \quad E \to E_0 \,. \tag{10}$$

4. Following a similar approach in three dimensions show that

$$\varrho(E) \to \begin{cases} +\dfrac{a^3}{\sqrt{2}\pi^2}\sqrt{\dfrac{E - E_0}{A_x A_y A_z}} + \text{const.} \quad \text{as } E \to E_0^{\pm} \,, & \text{(11a)} \\ -\dfrac{a^3}{\sqrt{2}\pi^2}\sqrt{\dfrac{E - E_0}{A_x A_y A_z}} + \text{const.} \quad \text{as } E \to E_0^{\pm} \,, & \text{(11b)} \end{cases}$$

where (11a) is for E_0 being an extremum (either minimum or maximum) while (11b) is for E_0 being a saddle point of $E\left(\boldsymbol{k}\right)$.
Note that if $\nabla_k E\left(\boldsymbol{k}\right)$ is zero along a line, then the 2-d singularity is as in 1-d. Similarly, if $\nabla_k E\left(\boldsymbol{k}\right)$ is zero along a line in 3-d, then the singularities are as in the 2-d case, and if $\nabla_k E\left(\boldsymbol{k}\right) = 0$ in a surface in 3-d, then the singularities are as in the 1-d case.
Apply (11a) and (11b) to sketch the shape of the DOS for the case of $E(k) = \varepsilon_0 + 2V\left[\cos(k_x a) + \cos(k_y a) + \cos(k_z a)\right]$.

5.9. Using (5.47) prove that $G(1; z) = B^{-1} - G(l, l; z)/\lambda$. Then show (5.39b).

Table 5.2. Numerical values for the simple cubic Green's functions $G(\ell_1 - m_1, \ell_2 - m_2, \ell_3 - m_3)$ [in units of $(2|V|)^{-1}$]

$E/2\|V\|$	$\mathrm{Re}\{G(0,0,0)\}$	$\mathrm{Im}\{G(0,0,0)\}$	$\mathrm{Re}\{G(1,0,0)\}$	$\mathrm{Im}\{G(1,0,0)\}$	$\mathrm{Re}\{G(1,1,0)\}$	$\mathrm{Im}\{G(1,1,0)\}$	$\mathrm{Re}\{G(1,1,1)\}$	$\mathrm{Im}\{G(1,1,1)\}$
0.0	0.0	0.896441	−0.333333	0.0	0.0	−0.185788	0.275664	0.0
0.2	0.074176	0.896927	−0.328388	0.059795	−0.036758	−0.183040	0.265774	−0.082250
0.4	0.152660	0.898396	−0.312979	0.119786	−0.073595	−0.174773	0.234932	−0.163723
0.5	0.195323	0.899508	−0.300780	0.149918	−0.092168	−0.168550	0.210461	−0.204031
0.6	0.241798	0.900881	−0.284974	0.180176	−0.111043	−0.160914	0.178622	−0.243895
0.8	0.356091	0.904444	−0.238376	0.241185	−0.151676	−0.141336	0.083045	−0.321774
1.0	0.642882	0.909173	−0.119039	0.303058	−0.239523	−0.115850	−0.201461	−0.396661
1.2	0.623924	0.617641	−0.083764	0.247056	−0.210658	0.000621	−0.195407	−0.152186
1.4	0.606577	0.506449	−0.050264	0.236343	−0.180223	0.049291	−0.183703	−0.073165
1.5	0.598434	0.463545	−0.034116	0.231772	−0.164446	0.067430	−0.175882	−0.043612
1.6	0.590611	0.425657	−0.018341	0.227017	−0.148310	0.082687	−0.166779	−0.018002
1.8	0.575841	0.360233	0.012171	0.216140	−0.115001	0.106135	−0.144801	0.024441
2.0	0.562116	0.303994	0.041411	0.202662	−0.080371	0.121426	−0.117903	0.057434
2.2	0.549312	0.253400	0.069496	0.185826	−0.044490	0.129014	−0.086194	0.081738
2.4	0.537326	0.205800	0.096528	0.164640	−0.007418	0.128408	−0.049765	0.096681
2.5	0.531612	0.182285	0.109677	0.151904	0.011546	0.124557	−0.029803	0.100026
2.6	0.526070	0.158374	0.122594	0.137257	0.030785	0.117828	−0.008689	0.099991
2.8	0.515470	0.105986	0.147772	0.098920	0.070069	0.092137	0.036969	0.085629
3.0	0.505462	0.0	0.172129	0.0	0.110383	0.0	0.087157	0.0
3.2	0.400104	0.0	0.093444	0.0	0.042757	0.0	0.025989	0.0
3.4	0.357493	0.0	0.071825	0.0	0.028498	0.0	0.015398	0.0
3.5	0.341048	0.0	0.064556	0.0	0.024187	0.0	0.012450	0.0
3.6	0.326621	0.0	0.058612	0.0	0.020855	0.0	0.010270	0.0
3.8	0.302143	0.0	0.049381	0.0	0.016041	0.0	0.007296	0.0
4.5	0.242855	0.0	0.030949	0.0	0.007868	0.0	0.002870	0.0

Table 5.2. (continued)

$E/2\,\lvert V\rvert$	$\mathrm{Re}\,\{G(2,0,0)\}$	$\mathrm{Im}\,\{G(2,0,0)\}$	$\mathrm{Re}\,\{G(2,1,0)\}$	$\mathrm{Im}\,\{G(2,1,0)\}$	$\mathrm{Re}\,\{G(2,1,1)\}$	$\mathrm{Im}\,\{G(2,1,1)\}$	$\mathrm{Re}\,\{G(2,2,0)\}$	$\mathrm{Im}\,\{G(2,2,0)\}$
0.0	0.0	−0.153291	0.057669	0.0	0.0	0.185788	0.0	−0.051116
0.2	−0.058501	−0.140847	0.055263	−0.014153	0.072194	0.172074	−0.035756	−0.041527
0.4	−0.108662	−0.103475	0.048608	−0.025972	0.136244	0.131113	−0.065024	−0.012416
0.5	−0.127430	−0.075392	0.044234	−0.030162	0.162322	0.100539	−0.074501	0.010095
0.6	−0.139596	−0.041012	0.039726	−0.032830	0.182491	0.063357	−0.078274	0.038275
0.8	−0.130786	0.046798	0.033989	−0.032481	0.195967	−0.030276	−0.054995	0.112685
1.0	0.077131	0.160342	0.081196	−0.022246	0.105070	−0.148591	0.169476	0.214911
1.2	0.017674	−0.027190	0.026381	−0.094125	0.054332	−0.122370	0.131214	−0.003198
1.4	−0.026422	−0.041854	−0.018346	−0.094170	0.008767	−0.117578	0.088374	−0.056319
1.5	−0.042997	−0.037947	−0.036071	−0.087016	−0.011436	−0.111042	0.066251	−0.070590
1.6	−0.056060	−0.029951	−0.052177	−0.076716	−0.029587	−0.101889	0.044256	−0.079012
1.8	−0.072019	−0.006670	−0.074373	−0.049538	−0.058760	−0.076806	0.002587	−0.081221
2.0	−0.074987	0.020951	−0.084251	−0.017244	−0.076833	−0.044847	−0.032527	−0.067062
2.2	−0.065573	0.048180	−0.081178	0.016267	−0.081929	−0.009132	−0.056640	−0.040003
2.4	−0.044321	0.070841	−0.064567	0.046857	−0.072205	0.026283	−0.064998	−0.004542
2.5	−0.029411	0.079009	−0.051010	0.059461	−0.061218	0.042154	−0.061705	0.014298
2.6	−0.011721	0.084050	−0.033863	0.069106	−0.045846	0.055489	−0.052563	0.032255
2.8	0.031780	0.079419	0.011450	0.073435	−0.001059	0.067703	−0.014039	0.056992
3.0	0.085779	0.0	0.071863	0.0	0.063931	0.0	0.056110	0.0
3.2	0.026911	0.0	0.017389	0.0	0.012685	0.0	0.009106	0.0
3.4	0.016927	0.0	0.009670	0.0	0.006405	0.0	0.004293	0.0
3.5	0.014093	0.0	0.007649	0.0	0.004862	0.0	0.003180	0.0
3.6	0.011965	0.0	0.006197	0.0	0.003792	0.0	0.002428	0.0
3.8	0.008988	0.0	0.004279	0.0	0.002443	0.0	0.001513	0.0
4.5	0.004213	0.0	0.001588	0.0	0.000743	0.0	0.000428	0.0

Table 5.2. (continued)

$E/2\lvert V\rvert$	$\mathrm{Re}\{G(3,0,0)\}$	$\mathrm{Im}\{G(3,0,0)\}$	$\mathrm{Re}\{G(3,1,0)\}$	$\mathrm{Im}\{G(3,1,0)\}$	$\mathrm{Re}\{G(4,0,0)\}$	$\mathrm{Im}\{G(4,0,0)\}$
0.0	0.102658	0.0	0.0	0.018619	0.0	0.078814
0.2	0.083937	−0.059520	0.008731	0.015606	0.057151	0.054616
0.4	0.031616	−0.098678	0.013680	0.007660	0.079233	−0.006106
0.5	−0.003588	−0.104662	0.013690	0.002605	0.069084	−0.039691
0.6	−0.041447	−0.098070	0.011602	−0.002458	0.043454	−0.066840
0.8	−0.106839	−0.036386	−0.000094	−0.009563	−0.039781	−0.066765
1.0	−0.051484	0.106611	−0.054831	−0.006713	0.039227	0.079732
1.2	0.020657	0.064189	0.016421	0.048606	−0.033782	−0.013180
1.4	0.049665	0.023146	0.049369	0.020362	−0.031992	0.025213
1.5	0.051810	0.002450	0.054050	0.002144	−0.017774	0.036722
1.6	0.047658	−0.015996	0.052321	−0.015436	−0.000717	0.040510
1.8	0.026051	−0.042000	0.034211	−0.042968	0.028959	0.027341
2.0	−0.004357	−0.049882	0.004549	−0.054598	0.039365	−0.002085
2.2	−0.033303	−0.038901	−0.026625	−0.047353	0.025540	−0.029932
2.4	−0.051000	−0.012029	−0.048773	−0.022359	−0.005390	−0.039145
2.5	−0.052691	0.005294	−0.053043	−0.004865	−0.021874	−0.033078
2.6	−0.048091	0.023380	−0.050898	0.014238	−0.034762	−0.019427
2.8	−0.015603	0.052086	−0.021571	0.047283	−0.032872	0.023128
3.0	0.055090	0.0	0.051046	0.0	0.040578	0.0
3.2	0.009231	0.0	0.007147	0.0	0.003578	0.0
3.4	0.004594	0.0	0.003231	0.0	0.001389	0.0
3.5	0.003499	0.0	0.002360	0.0	0.000962	0.0
3.6	0.002749	0.0	0.001782	0.0	0.000695	0.0
3.8	0.001809	0.0	0.001091	0.0	0.000396	0.0
4.5	0.000611	0.0	0.000299	0.0	0.000094	0.0